Recent Advances in the Applications of Mesoporous Silica in Heterogenous Catalysis

Journal:	*Catalysis Science & Technology*
Manuscript ID	CY-MRV-01-2022-000001.R1
Article Type:	Minireview
Date Submitted by the Author:	08-Jun-2022
Complete List of Authors:	Yu, Xinbin; University of South Carolina, Chemical Engineering Williams, Christopher; University of South Carolina, Chemical Engineering

SCHOLARONE™
Manuscripts

Recent Advances in the Applications of Mesoporous Silica in Heterogenous Catalysis

Xinbin Yu[1] and Christopher T. Williams[1]*

[1]Department of Chemical Engineering, University of South Carolina, Columbia, SC 29208 USA

*Correspondence: willia84@cec.sc.edu

Abstract

Mesoporous silica is a class of silica material with a large specific surface area, high specific pore volume and meso-sized pores. These properties make mesoporous silica a good choice of support in heterogeneous catalysis. In this review, we discuss the functionalization of mesoporous silica, preparations of mesoporous silica supported catalysts and their typical applications in heterogenous catalysis. We highlight the introduction of different functionalities over mesoporous silica and their cooperation to achieve the catalytic turnover. Both the advantages and disadvantages of mesoporous silica as support in these applications are compared, such as regulating the particle size distribution, dispersion of active species and interaction between active species-support. The review aims to summarize the recent progress on mesoporous silica related catalytic applications and provide valuable insight into the rational design of efficient catalysts.

Keywords Mesoporous silica, support, catalysis, functionalization.

1. Introduction

The production of chemicals (*e.g.* fuels, bulk chemicals, fine chemicals, and pharmaceuticals) *via* catalytic process consumes nearly 25% of the energy used in industry.[1,2] Heterogeneous catalysts refer to catalytic materials existing in solid phase different from the reactants and products in gas and/or liquid phases. They are widely applied in industrial processes, such as ammonia synthesis, dehydrogenation/hydrogenation, hydrocarbon cracking, and oxidation, to name a few. The active sites in heterogeneous catalysts are often the defects (*e.g.* terraces, steps, kinks, and corners) in the scale of nanometers on the surface. Suitable support materials are typically employed to increase the number of active sites and introduce necessary functionalities to the catalysts, which is particularly important for precious metal catalysts due to the concern of costs.

The most important concern about support materials is their stability in high temperature reactions. Due to the excellent stability at high temperature, many materials (*e.g.* Al_2O_3, SiO_2, CeO_2, ZrO_2, TiO_2, Al_2O_3-SiO_2, C, *etc.*) are exploited as support in heterogeneous catalysis depending on the requirements of reactions. Numerous studies indicate that the characteristics of supports such as acid/base properties, morphologies and pore structures have a significant effect on the catalytic performance. Among various support materials, silica is usually regarded as the simplest one and has many applications. The commonly used silica supports (*e.g.* silica gel, colloidal silica, ordered mesoporous silica) are amorphous in nature, with types of silanol groups and siloxane bridges on the surface as shown in Figure 1.[3] Unlike many supports, silica is usually considered as neutral and further modification of the surface can incorporate different functionalities such as acid/base sites.

Figure 1. Types of silanol groups and siloxane bridges on the surface of amorphous silica, and internal OH groups, Q^i -terminology is used in NMR, where n indicates the number of bridging bonds (-O-Si) tied to the central Si atom: Q^4, surface siloxanes; Q^3, single silanols; Q^2, geminal silanols (silanediols). (Reproduced from ref. 3 with permission from Elsevier, copyright 2000)

Conventional silica is usually produced by mixing sodium silicate and mineral acid to form monomeric silicic acid followed by its condensation polymerization and subsequent treatments. It has ill-defined, intra-particle pores resulting from the accumulation of solid particles.[4] The specific surface area, pore diameter and pore volume can be regulated in a large range. In 1992, Kresge *et al.* from

ExxonMobil first reported the preparation of ordered mesoporous silica by using multimolecular templates.[5] The material was named MCM-41, which had uniform, regularly arranged pores with 3-10 nm in diameter. In 1998, Zhao *et al.* increased the diameter of mesopores to 30 nm by using polymeric surfactants.[6] The prepared SBA-15 material had a thicker amorphous silica wall compared to MCM-41, which enhanced the thermal and hydrothermal stability. Since then many more ordered mesoporous silica (*e.g.* FDU, HMS, MSU, KIT, *etc.*) were prepared with different diameters, shapes and connectivity of the pores and mesoporous silica nanoparticles.

The common features of mesoporous silicas are: (1) high specific surface area (up to 2370 m^2/g), (2) high specific pore volume (up to 1.4 cm^3/g); (3) uniform pores and narrow pore size distributions (Figure 2).[7,8] These characteristics enable mesoporous silicas to be excellent supports for active sites in heterogeneous catalysts. The high specific surface area and specific pore volume facilitate the dispersion of metals or metal oxides, which is a key aspect in many reactions. The mesopores could serve as host for metal particles and confine their growth at high temperatures when the particles are loaded inside the channels. This characteristic is particularly important as the sintering of particles is one of the most significant problems of high temperature catalytic reactions.[9,10,11,12] Hence, many methods are developed to load particles inside the mesopores. Like other types of silica, mesoporous silica is considered as neutral. The acid/base property could be introduced by incorporating other species such as Al^{3+} for target applications.
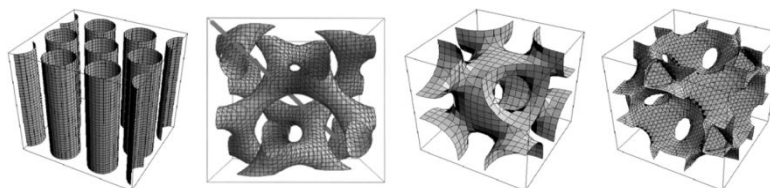
Figure 2. Structure of the four synthesized OMS. Starting from the left, SBA-15 (p6mm), KIT-6 (Ia-3d), SBA-16 (Im-3m) and FDU-12 (Fm-3m). (Reproduced from ref. 13 with permission from Elsevier, copyright 2008)

Several reviews about mesoporous silica have been published in recent years. For example, Liang *et al.* compared the catalytic activities among zeolites, mesoporous silica, and metal-organic frameworks (MOFs).[14] Gérardin *et al.* discussed the strategies for synthesis of mesoporous silica materials *via* environmentally friendly and economical routes.[15] Singh *et al.* reviewed the synthesis of SBA-15 supported catalysts for reforming.[16] This mini review focus on the surface functionalization of mesoporous silica, synthesis of mesoporous silica and mesoporous silica nanoparticles supported catalysts and their applications in several reactions.

2. Surface Engineering of mesoporous silica

To broaden the application of mesoporous silica, surface engineering is conducted to incorporate necessary surface moieties (organic functional groups and dispersed metal particles) as the bare silica surface only has a limited amount of -OH. Many functional groups, such as -COOH, -CN, -NH$_2$, -SH, -SO$_3$H, have been introduced to the surface of mesoporous silica successfully, either through co-condensation during the synthesis or by post-synthesis grafting (**Table 1**).[17,18,19,20,21] In the co-condensation method, organosilanes and silica precursors are copolymerized and template materials are removed by chemical extraction to keep the functional groups intact. It can also achieve a

high loading of organic functional groups. Chen *et al.* prepared SBA-15 functionalized with –COOH by dropping a mixture of tetraethoxysilane (TEOS) and carboxyethylsilanetriol sodium salt (CES, 25 wt% in water) into the solution of Pluronic P123 and HCl.[22] Post-synthesis grafting method uses silanols as anchor points but the calcination process prior to grafting may reduce the surface density of Si-OH.[23] Moreover, the organic functional groups are found not homogeneously grafted over the surface, since the external surface and pore entrances are more kinetically accessible than the internal surface.[24,25] Ganji *et al.* fabricated SBA-NH_2 by refluxing a mixture of (3-Aminopropyl) triethoxysilane (APTES, 3 mL), SBA-15 (1 g) and dry toluene (30 mL) in N_2 atmosphere for 24 h. Elemental analysis revealed that the amount of nitrogen was 1.2 mmol/g.[26] Bagheri *et al.* synthesized KIT-6-SH, SBA-15-SH, MCM-41-SH by refluxing a mixture of ordered mesoporous silica (1.0 g), toluene (50mL) and 3-(trimethoxysilyl)-1-propanethiol (2.0g) for 12h.[27]

Table 1. Examples of mesoporous silica functionalized with different moieties

Functional group	Materials	Preparation method	Specific surface area(m^2/g)	Pore size(nm)	Pore volume(cm^3/g)	Ref.
-CN	SBA-15	Co-condensation	~	~	~	28
-SH	SBA-15	Post-synthesis	636	7.1	0.77	29
-COOH	SBA-16	Co-condensation	664	7.7	0.68	30
-SO_3H	HMS	Co-condensation	331	3.6	0.10	31
		Post-synthesis	1045	2.6	0.65	
Al^{3+}	SBA-15	Co-condensation	1004	7.4	1.53	32
	SBA-15	Co-condensation	1023.9	7.4	1.28	33
	SBA-15	Co-condensation	701	7.7	0.70	34
	MCM-41, MCM-48, SBA-1, KIT-1, and MSU-1	Post-synthesis	~	~	~	35
-NH_2	SBA-15-$(CH_2)_2$-NH_2	Co-condensation	570	5.24	0.75	25
-NHR, -NRR	MCM-41	Post-synthesis	~	~	~	36
K^+	SBA-15	Impregnation	~	~	~	37
Ba^{2+}	MCM-41	Co-condensation	~	~	~	38
Mg^{2+}	MCM-41	Hydrothermal method	~	~	~	39
Ca^{2+}	SBA-15	Hydrothermal	395	9.4	0.70	40
-SO_3H and -NH_2	Mesoporous silica nanoparticles	Co-condensation and Post-synthesis	934	2.6	0.89	41

Al^{3+} and Mg^{2+}	SBA-15	Hydrothermal method	~	~	~	42

Some researchers have developed surface grafting of organic functionalities with simultaneous extraction of the surfactant. Antochshuk *et al.* reported the use of silane to react with silanols and displace the surfactant in the as-synthesized silica-surfactant materials.[43] The template materials could be displaced by almost any silane with at least one "reactive group" (Cl-, EtO-, or MeO-).[44] They prepared MCM-41 and Ce-MCM-41functionalized with octyl, cyanopropyl, aminopropyl and mercaptopropyldimethoxysilyl groups *via* this method. Liu *et al.* modified the procedures by using alcohol as the solvent to extract surfactant and graft silanes simultaneously.[23] This was found to increase the amount of attached silane on the surface and produce a more uniform and well-controlled monolayer.

Interests are growing in selective functionalization of the internal and external surfaces of mesoporous silica. Selectively functionalizing the external surface can influence the interaction between the silica particles with the surrounding environment, while functionalizing the internal surface aims to facilitate the introduction of other species (e.g., metal ions, metal nanoparticles) inside the channels. Kecht *et al.* developed a sequential, site-selective co-condensation approach that allowed the selective functionalization depending on the time of addition of the organosilanes during the growth of particles.[45] The density of functional groups on the external surface could be regulated by changing the organosilane-to-TEOS ratio.
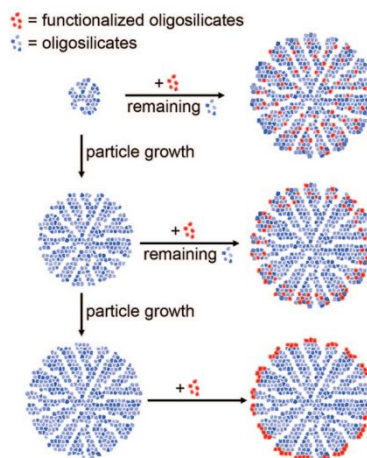
Scheme 1. Distribution of functional groups depending on the addition time of the organosilane component during synthesis. (Reproduced from ref. 45 with permission from American Chemical Society, copyright 2008)

An ordered mesoporous silica, such as SBA-15, usually contains a significant amount of micropores due to the hydrophilic EO chains buried in the silica matrix at the synthesis stage. Selective surface functionalization of the micropores or mesopores is therefore proposed. Yang *et al.* took advantage of different locations of templates (in the mesopores or buried in the silica matrix) on mesoporous silica SBA-15 and their reactivity to sulfuric acid to selectively decompose the templates in the mesopores first.[46,47] Then the mesopore surface and

external surface were functionalized with trimethylchlorosilane (TMCS). The templates in the micropores were removed by heating the

material at 250 °C while trimethylsilyl (TMS) groups were kept intact. The fresh micropores were subsequently functionalized with

trivinylchlorosilane (TVCS) to create difference among micropore surface, mesopore surface and external surface.
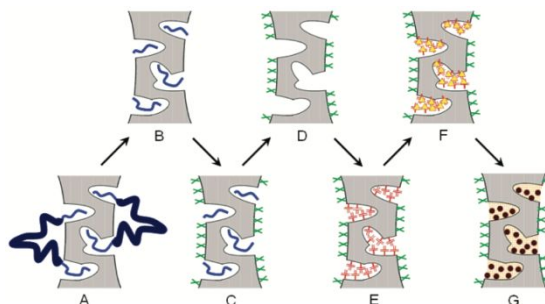
Scheme 2. Schematic representation of selective surface functionalization of SBA-15, A. as-synthesized SBA-15, B. H_2SO_4 treated SBA-

15, C. TMCS functionalized SBA-15, D. SBA-15 with templates in the micropores removed, E. TVCS functionalized SBA-15, F. metal

salt-incorporated material, G. sample containing reduced metal. (Reproduced from ref. 46 with permission from American Chemical

Society, copyright 2007)

One advantage of mesoporous silica over zeolites is the much larger diameter of pores, which allows the efficient diffusion of bulky

molecules, such as the heavy fractions in crude oil. However, due to the lack of Al^{3+}, the acidity (strength and amount) of mesoporous

silica is much weaker than zeolites and acidity is key to many reactions (*e.g.* cracking, isomerization, dehydration). Thus, many efforts are

devoted to incorporating Al^{3+} species into mesoporous silica.

Directly introducing Al^{3+} and other metal ions onto the framework of mesoporous silica is very difficult due to the decomposition of metal-

O-Si in the highly acidic conditions typically employed for the synthesis of mesoporous silica.[33] In the case of Al^{3+}, the hydrolysis rates of

aluminum alkoxides are significantly higher than that of silicon alkoxides.[48] Yue *et al.* prepared Al-SBA-15 by hydrolysis of tetraethyl

orthosilicate (TEOS) and aluminum tri-tert-butoxide in HCl solution first and then added templates (in HCl solution) followed by further

treatment.[32] The control of preparation conditions was vital to the incorporation of Al^{3+}.[49] Li *et al.* used aluminum isopropoxide as Al^{3+}

source and TEOS (fluoride was used to accelerate the hydrolysis rate) or TMOS as the Si^{4+} source in acidic condition to synthesize Al-

SBA-15.[33] By adjusting the pH of solution and the sequence of mixing to control the hydrolysis, Al-SBA-15 with high quality was obtained

(Figure 3). Wu et al. took advantage of the self-generated weak acidity in the aqueous precursor solution (TEOS, P123, $Al(NO_3)_3$) and

prepared plugged Al-SBA-15 (Al/Si molar ratio: 0.25-4) in the absence of mineral acid at at 45 °C.[34] The incorporation of Al^{3+} not only

induced acidity but also increased the wall thickness. The weak acidity slowed down the rates of precursor hydrolysis and condensation,

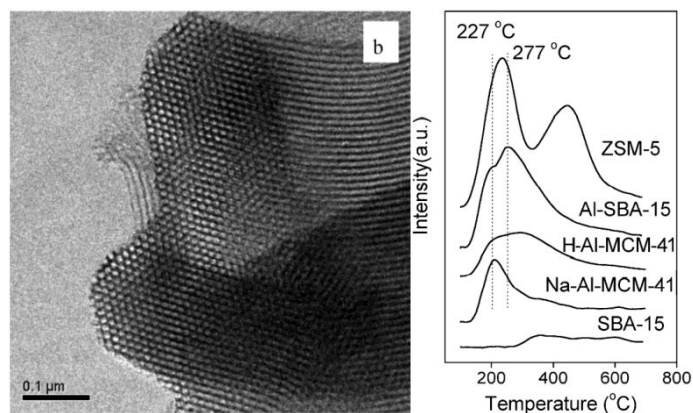which resulted in the formation of plugs structure.

Figure 3. TEM images of calcined Al-SBA-15 (Si/Al = 20) in the direction of the pore axis. NH_3-TPD profiles of Al-SBA-15 (Si/Al = 10), SBA-15, Na(H)-Al-MCM-41 (Si/Al = 10), and ZSM-5 (Si/Al = 50). (Reproduced from ref. 33 with permission from American Chemical Society, copyright 2004)

Post-synthesis is also a common method to graft Al^{3+} onto mesoporous silica. The Al^{3+} is first grafted onto silanol groups on the silica framework in liquid phase and subsequent calcination might incorporate Al^{3+} into the silica framework *via* thermal activation.[35] Mokaya *et al.* reported the synthesis of Al-MCM-41 by reacting calcined MCM-41 with solution of aluminum chlorohydrate at 80 °C followed by subsequent treatment.[50] Ryoo *et al.* incorporated Al^{3+} to ordered mesoporous silica (MCM-41, MCM-48, SBA-1, KIT-1, and MSU-1) by mixing them into nonaqueous (*e.g.* ethanol) solutions of $AlCl_3$ or $Al(NO_3)_3$ at 20-60 °C.[35] The Al^{3+}-containing products could be obtained after washing, drying and calcination. Zeng *et al.* prepared Al-SBA-15 by hydrolysis of $AlCl_3$ with aqueous TMAOH (tetramethylammonium hydroxide) first followed by mixing calcined SBA-15 with the solution and further treatments.[51] Ti^{4+}, Sn^{2+}, Zn^{2+} and Mn^{4+}-modified ordered mesoporous silica could also be prepared by post-synthesis method.[35,52,53]

Other metal oxide species can be loaded on/into silica wall by co-condensation and post synthesis as well.[54,55] The metal oxide-incorporated mesoporous silica is extensively applied in various reactions due to the enhanced dispersion of metal oxide. It is particularly beneficial to noble metal catalysts as the interaction between metal and metal oxide can be enhanced.[56] Zhang et al. incorporated 10 wt% Nb into the framework of mesoporous silica *via* micellar templating method.[57] They took advantage of the slow condensation of silicate at low temperature to form loosely-bonded silica gel which could bond with heteroatom precursors. Subsequent high temperature hydrothermal treatment could further condense the Nb polyanions into the framework of silica. Using sodium silicate rather than TEOS as silicon source could result in more Nb species incorporated in the wall as hydrolysis and condensation rates of sodium silicate better match with the fast hydrolysis of $Nb(OEt)_5$. Chen et al. incorporated molybdenum species onto the pore wall of KIT-6 *via* a one-pot co-assembly method.[58] In this process, silicates assemble with molybdate oligomers in the presence of surfactant to incorporate Mo species into the silica wall. The microporosity is kept and the pore sizes gradually increase with the elevating Mo loading, possibly due to the substitution of Si by Mo in the framework. Besides, Shi et al. developed a dissolution-regrowth" strategy to prepare various metal-doped (*e.g.* Fe, Cu, Mn, Mg, Ca) mesoporous silica.[59] Mesoporous silica nanoparticles were first dissolved into oligomers by strong bases. Then the oligomers react with metal-containing precursors to construct Si-O-M (M: metal dopants) framework and form a metal-doped nanoparticle with hollow structure.

For mesoporous silica support metal/metal oxide particles, one important topic is increasing the dispersion. It can be achieved by choosing an appropriate catalyst preparation method (e.g. impregnation, precipitation, atomic layer deposition, strong electrostatic adsorption, one-pot co-condensation) or loading suitable promoters for the main components.[60,61,62,63,64,65,66,67] Recently, it has been shown that adding modifying agents (e.g. P123, PVP, β-cyclodextrin, CTAB, ethylene glycol, oleic acid, EDTA) to the precursors solution before impregnation can improve the dispersion of metal species.[68,69,70,71,72] Yang et al. comprehensively studied the role of P123 in enhancing the dispersion of Ni over SBA-15 prepared by impregnation.[70] Raman and FTIR results indicated that P123 could form crown-ether-type complex with Ni^{2+}, NO_3^- and H_2O in the sample drying stage. The strong interaction between Ni and P123 not only facilitated the dispersion of $Ni(NO_3)_2 \cdot 6H_2O$ but also inhibited the migration of $Ni(NO_3)_2 \cdot 6H_2O$ out of the mesopores. As the as-synthesized mesoporous silica contains a large amount of organic templates which occupy the mesopores, removal of templates by calcination is commonly conducted before loading other species. Yue et al. showed that there was nano-confined space between templates and the silica wall to accommodate other species.[73] Recently, nanoconfinement effect utilizing the nano-confined space and the abundant -OH in the as-synthesized mesoporous silica was developed to prepare SBA-15 supported highly dispersed Ni, Pd, Pt, Au, Rh, CeO_2, Co_3O_4 containing materials.[9,10,11,74,75,76,77] In a typical synthesis, the metal precursor was first finely grinded and then grinded with the template-containing SBA-15 for a certain amount of time (Scheme 3). Then the mixture was calcined to remove template and obtain the oxidized catalysts. Compared with catalysts prepared with templated-free SBA-15, the dispersion of metals is significantly improved over the catalysts derived from template-containing SBA-15.
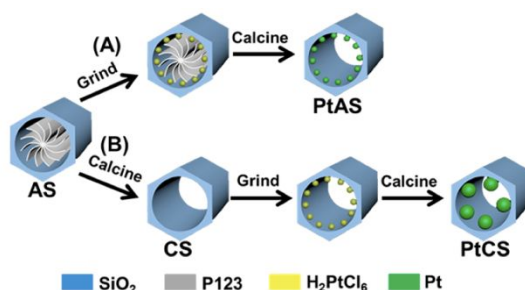
Scheme 3. Formation of (A) Small-Size Pt NPs in Confined Spaces and (B) Large-Size Pt NPs in Conventional Mesoporous Silica. (Reproduced from ref. 11 with permission from American Chemical Society, copyright 2018)

The generation of basicity over mesoporous silica could be achieved by incorporation of certain metal oxides (*e.g.* Ce, Mn, Mg, K_2O, CaO).[77,78,79,80,81,82,37] The low-temperature (< 70 °C) CO_2 desorption peaks from CO_2-TPD results indicated that weak basic sites were present on MnO_x and CeO_2 incorporated HMS and MCM-41.[83] For mesoporous silica with super-basicity, it was found that the composition of group 2 metal nitrates occurred at much lower temperature than that of group 1 metal nitrates. Thus, the meso-structure could be preserved when decomposing group 2 metal nitrates. However, the meso-structure collapsed when anneal group 1 metal nitrates at decomposition temperature directly. To solve this problem, various compounds (e.g. ZrO_2, C, methanol, MgO) were used to facilitate the

decomposition of group 1 metal nitrates or protect the meso-structure.[81] Sun et al. proposed a method to prepare ordered mesoporous silica with strong, basic sites.[84] They calcined the as-prepared SBA-15 in N_2 to decompose the templates into a carbon layer. Then $LiNO_3$ was impregnated onto C-coated SBA-15. Due to the existence of the carbon layer, the decomposition temperature of $LiNO_3$ decreased from 600 °C to 400 °C, which preserved the ordered meso-structure. The highest CO_2 desorption peak was located at 720 °C, proving the presence of strong, basic sites. Zhu et al. developed a redox strategy to generate strong basicity on mesoporous silica.[85] They first impregnated SBA-15 with KNO_3 solution followed by calcining the KNO_3-containing SBA-15 with methanol/N_2 stream at 400 °C. Without methanol, FTIR indicated that KNO_3 decomposed at temperature around 600 °C, which also caused the collapse of the meso-structure. In the presence of methanol, KNO_3 could decompose to K_2O at 400 °C facilely. CO_2-TPD revealed that the density of basic site was 1.87 mmol/g on the sample treated with methano/N_2 at 400 °C for 2 h, which was close to the theoretical value achieved when KNO_3 completely decomposed (1.98 mmol/g^{-1}).

Typical organic base functionalities that can be incorporated onto mesoporous silica are -NH_2, NHR, NR_2, piperazine and guanidine via co-condensation or post-synthesis method. [25,86, 87,88,89,36,90] The differences in the amount and location of amino groups over MCM-41 materials synthesized by co-condensation or post-synthesis grafting were compared by Yokoi et al.[89] A detailed review of the generation of basicity over mesoporous material was provided by Sun et al.[91] Moreover, the as-prepared amino-functionalized mesoporous silica can be used to anchor other metal complexes or particles (e.g. Cu, Au) to extend the applications.[92]

It is viable to functionalize the surface of mesoporous silica with both acidic and basic groups.[21,93,94] The -SO_3H and -NH_2 co-functionalized mesoporous silica synthesized through one-pot co-condensation methods under basic condition. The as-synthesized material was treated with HCl/EtOH (0.3 g/100 mL) at 60 °C for 6 h to extract the template and generate SO_3H from SO_3Na.[95] Preparation of -COOH and -NH_2 co-functionalized mesoporous silica by grafting and co-condensation was also reported.[94] To selectively functionalize the internal and external surface, the general strategy is loading one functionality onto the internal surface *via* co-condensation followed by grafting the other group onto the external surface. Huang et al. prepared mesoporous silica nanoparticle with the internal surface and external surface functionalized by sulfonic acid (SO_3H) and amine groups (NH_2), respectively.[41] They first prepared mesoporous silica with -SH attached to the internal surface. Then they functionalized the external surface of template-containing silica with -NH_2 because of the protection of the internal surface by template. Finally, the -SH group could be converted to -SO_3H in a mixture of acetic acid and H_2O_2 at 100 °C for 6 h. Mesoporous silica nanoparticle with the internal surface functionalized by -NH_2 and external surface functionalized -SO_3H was synthesized by the same method. Inorganic, acid, and base functionalities can be co-incorporated onto mesoporous silica as well. Shi *et al.* introduced Al^{3+} and Mg^{2+} to SBA-15 in one pot under strong acidic condition.[42] The density of -OH on SBA-15 increased from 0.6 mmol to 4.3 mmol/g upon the introduction of Al^{3+}, indicating that Al^{3+} was inserted into the framework of SBA-15. CO_2-TPD revealed that the density of basic sites increased from 0.07 mmol/g to 1.10 mmol/g over Mg-loaded SBA-15. The strength of basicity (H_-) was 22.3 and the generation of basicity was assigned to the highly dispersed MgO.

3. Applications of mesoporous silica in heterogeneous catalysis

3.1 CO_2 hydrogenation

Hydrogenation of CO_2 to hydrocarbons (*e.g.* CH_4) and oxygenates (*e.g.* CH_3OH, $HCOOH$) is considered as a promising way for fixation and recycling of CO_2.[96,97] CH_4 is regarded as a cleaner fuel than coal. Moreover, the storage and transportation of CH_4 through the existing natural gas facilities are much easier compared to H_2. Both CH_3OH and $HCOOH$ are valuable raw materials for the synthesis of a variety of chemicals in industry.[98]
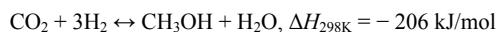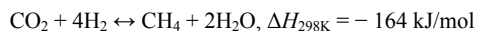
$$CO_2 + 4H_2 \leftrightarrow CH_4 + 2H_2O, \Delta H_{298K} = -164 \text{ kJ/mol}$$

$$CO_2 + 3H_2 \leftrightarrow CH_3OH + H_2O, \Delta H_{298K} = -206 \text{ kJ/mol}$$

Table 2. Applications of mesoporous silica-based catalysts in CO_2 hydrogenation.

Materials	Preparation method	Specific surface area (m^2/g)	Pore size (nm)	Pore volume (cm^3/g)	Catalytic reactions	Reaction conditions	Key results	Ref.
Pd_xCo_{1-x}@MSN	One-pot ligand-protected synthesis	601	2.9	0.73	CO_2 hydrogenation to formate	2 mL of H_2O containing 2 mmol of $NaHCO_3$, 10 mg catalyst, 2.0 MPa H_2 at 100 °C.	Formate formation rate: 408 $mol_{formate}/(mol_{total\ Pd} \cdot h)$ over Pd0.8Co0.2@MSN	97
Ru@MCM-3	Co-condensation	36	~	0.1	CO_2 hydrogenation to formic acid	10 mg of catalyst, 0.9 g TEA, 6 g water, 90 °C, reaction time: 15 h, 5 bar of CO_2 and 30 bar of H_2	TON=1500 over 3.2wt% Ru@MCM-3	99
FeCu/MCM-41	Impregnation	873	3.0, 17.4	0.79 (small size pore) 1.01 (large size pore)	CO_2 hydrogenation to alcohols	0.5 g of catalyst, CO_2/H_2 = 1:3, 200 °C, P=10 bar, GHSV = 4800 mL/(h·g_{cat})	CO_2 conversion = 2 %, alcohol selectivity =100 % over 3wt%Fe10wt%Cu/MCM-41	100
CuLa/SBA-15	Impregnation	470.3	5.3	0.58	CO_2 hydrogenation to methanol	240 °C, 3.0 MPa, H_2:CO_2:N_2 = 72:24:4, and GHSV = 12,000 mL/(g-cat·h).	CO_2 conversion = 5 %, methanol selectivity up to 81.2% over	101

							Cu1La0.2/ SBA-15	
Cu/ZnO/ ZrO$_2$@S BA-15	Im-pregnation-sol-gel autocombus tion	433	6.4	0.73	CO$_2$ hydrogenation to methanol	250 °C, 3.0 Mpa, GHSV= 44,000 cm^3/(h·g$_{cat}$), m$_{cat}$ = =0.45 g, H$_2$/CO$_2$ = 3	STY (MeOH) (g/g$_{cat}$/h) = 0.376, CO$_2$ conversion = 19.2%, methanol selectivity =30.60% over CZZS_20_ 1	102
Ni/SBA-16	Impregnatio n	231	4.9	0.24	CO$_2$ methanation	H$_2$/CO$_2$ =1:1, total flow rate = 30 mL/, 50 mg of catalyst 500 °C	CO$_2$ conversion =31%, CH$_4$ selectivity =33% over 21.7% Ni/SBA-16	30
Y$_2$O$_3$-Ni/MgO-MCM-41	Co-condensatio n	445	3.4 1	0.82	CO$_2$ methanation	H$_2$/CO$_2$ =4, GHSV = 9 L/(g$_{cat}$·h) and P= 1 atm, 400 °C	CO$_2$ conversion = 65.55%, CH$_4$ selectivity =84.44% over 2wt%Y$_2$O$_3$ -Ni/MgO-MCM-41	103
Ni/@Zr @MCM-41	Hydrotherm al method	643	3.9	0.74 8	CO$_2$ methanation	GHSV =6420 mL/(h·g$_{cat}$). flowrates of CO$_2$, 280 °C, 1 MPa, H$_2$ and N$_2$ are 20 mL/min, 80 mL/min and 7 mL/min, respectively.	CO$_2$ conversion = 88.6 %, CH$_4$ selectivity = 96.5 % over Ni/@Zr(0. 01)@MC M-41	104
Ni-La$_2$O$_3$/SB A-15	Citrate complex method	247	7.0	0.56	CO$_2$ methanation	H$_2$/CO$_2$ = 4:1, 1 MPa, 7 vol % N$_2$, 6000 mL/(h·g)	CO$_2$ conversion = 90.7% and CH$_4$ selectivity = 99.5% at 320 °C	105

1

Co/SBA-15	Atomic layer deposition	400-650	7.4-9	0.5-1.2	CO_2 hydrogenation to CO	600 °C, 0.1 MPa, $O_2/H_2/Ar$ = 45:45:10, GHSV $(mL/g_{cat.}/h)$= 18000	CO_2 conversion =37%, CO selectivity = 99.3% for 500 h over 2.6wt% Co/SBA-15	106

Supported noble metals (*e.g.* Pd, Ir, Ru, Rh) and some base metals (*e.g.* Ni, Fe, Cu, Co) catalysts are extensively investigated for the hydrogenation of CO_2 in literature (**Table 2**).[107] The reactions happen at relatively high temperature, which causes the sintering of metal particles and the subsequent decrease in the catalytic performance. Depositing the metallic particles into the pore channels of mesoporous silica is proposed to restrict the growth of particles. A variety of mesoporous silica (MCM-48, MCM-41, SBA-15 and MSU-F) supported Pd catalysts were prepared by incipient wetness impregnation method and tested for the hydrogenation of CO_2 in a flow reactor.[108] The analysis of Pd-Pd coordination number revealed that the average diameter of Pd^0 particles over catalysts with SBA-15 as support was less than 50% of the average diameter of Pd^0 over the amorphous silica supported catalysts. Moreover, the diameter of Pd^0 over silica supported catalysts was smaller than the pore sizes of the support, indicating that most of the Pd^0 could be deposited within the pores. The small mesopores of the mesoporous silica served as template for hosting Pd particles. Due to the poor stability of MCM silica, the pore systems of MCM-41 and MCM-48 changed during the preparation of catalysts. Further incorporating appropriate amount of Ca and K onto the catalysts dramatically increase the formation rate of CO and CH_3OH. In the case of Ca promoted 4 wt% Pd/SBA-15, the Pd-time yield of CH_3OH $(mol_{methanol} \cdot mol_{Pd}^{-1} \cdot s^{-1})$ reached the maximum when Ca/Pd molar ratio was 0.4–0.5. Increasing the loading amount of Ca caused the blockage of mesopores by Ca, leading to the inaccessibility of certain amount of Pd^0 for decomposing H_2.

Pd, NiPd and Ni particles were prepared by wet chemistry in solvent first and then loaded onto SBA-15 in solvent with ultrasonic stirring.[109] The catalysts were tested in a flow reactor for hydrogenation of CO_2 to CH_4. CO_2 conversion of 96.1% and a CH_4 yield of 93.7 % was obtained over $Ni_{0.75}Pd_{0.25}$/SBA-15 catalyst at 430 °C and GHSV of 6000 ml/(g·h). The particle sizes of all catalysts were around 6 nm which ruled out the effect of particle size on the performance. The synergistic effect between Pd and Ni was attributed to electron transfer from Pd to Ni, increasing the electron density of Ni for activation of CO_2 and dissociating intermediates to CH_4.

Due to abundance of base metals, mesoporous silica supported base metal catalysts are applied to the hydrogenation of CO_2. Many studies find that nickel catalysts are highly active for the formation of CH_4. However, the sintering of Ni particles restricts the industrial applications. Moreover, CO_2 hydrogenation over Ni catalysts is structure sensitive.[110,111,112] Thus, the choice of support material is important to the Ni catalysts. $Ni-La_2O_3$/SBA-15 catalysts were prepared by citrate complex method and tested for the CO_2 methanation in a flow reactor.[105] The citrate complex method facilitated the formation of $LaNiO_3$ with perovskite structure after calcination and the reduction of this species lead to Ni particles with diameter smaller than 5 nm, which was much smaller than the diameter of Ni particles prepared by impregnation method. The La_2O_3 species not only alleviated the sintering of Ni by strongly interacting with Ni species but

also promoted the adsorption of CO_2 at elevated temperature. CO_2 conversion of 90.7% and selectivity to CH_4 of 99.5% were achieved over 10 wt% Ni-La_2O_3/SBA-15 at 320 $^\circ$C. Ni particles can also be encapsulated in mesoporous silica by a two-step method.[113] The first step is the preparation of colloidal Ni nanoparticles with controllable size and the second step is the *in situ* hydrolysis of TEOS to form mesoporous silica in the presence of Ni nanoparticles. The mesoporous silica encapsulated Ni catalysts were thermally stable for 70 h at 350 °C. Moreover, the diameter of mesopores strongly influence the diameter of the Ni particles as Ni species were redistributed inside the mesopores under oxidation-reduction pretreatments.

Ordered mesoporous silica with short-channel, platelet morphology is employed as support for Ni catalysts to overcome the growth of metal particles into nanorods inside the long mesopore channels, which blocks the pores. 3 wt% Ni/p-SBA-15 (platelet SBA-15) was prepared by impregnation method and tested for CO_2 methanation in a flow reactor.[114] The Ni particle size was around 3 nm over 3 wt% Ni/p-SBA-15, which was much smaller the Ni particle size (7 nm) over 3 wt% Ni/SBA-15 (Figure 4). The interaction between Ni and the Si-OH groups of p-SBA-15 may create strongly adsorbing sites for CO and CO_2 on the catalysts, which facilitates the hydrogenation of CO_2 to CH_4 with CO from reverse water-gas shift reaction as the intermediate.
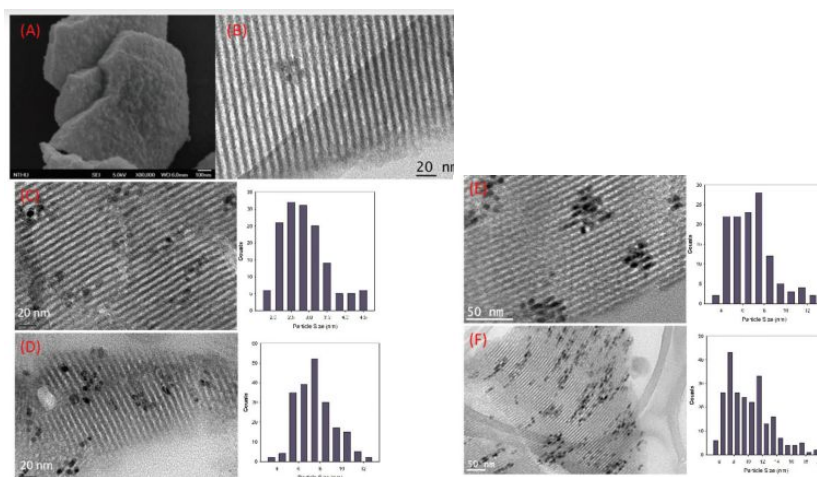
Figure 4. (A) SEM and (B) TEM images of the p-SBA-15 sample; TEM images and particle distribution of (C) the 3 wt% Ni/p-SBA-15 sample; (D) the 5 wt% Ni/p-SBA-15 sample; (E) the 3 wt% Ni/SBA-15 sample and (F) the 5 wt% Ni/SBA-15 sample. (Reproduced from ref. 114 with permission from The Royal Society of Chemistry, copyright 2019)

Ordered mesoporous silica with other symmetries in pore structure is also studied as a support in the hydrogenation of CO_2. Ni supported on SBA-16 with 3D cage structure was prepared by impregnation method at pH = 9 followed by calcination in air and reduction in H_2 at 500 $^\circ$C.[115] Ni^{2+} ions were electrostatically immobilized over the negatively charged silanols on the surface of silica. The high specific surface area and cage structure of SBA-16 help disperse Ni particles and confined their growth in size. For Ni/SBA-16 with metal loading of 5.8, 12.9 and 22.9 wt%, the Ni particle sizes were all around 4 nm. In comparison, the Ni particle sizes over regular SiO_2 (surface area= 300 m^2/g) supported Ni catalysts with metal loading of 3.3, 5.6, 12.0 wt% were 6.5, 7.4, 8.9 nm, respectively. The reaction proceeded as $CO_2 \rightarrow CO \rightarrow CH_4$. Unlike the high selectivity to CO over supported metal catalysts with small particle sizes, the Ni/SBA-16 catalysts with

small particle sizes were more selective to the formation of CH_4, which might result from the higher coverage of H_2 over the Ni surface. To better regulated the Ni particle sizes over SBA-16, -COOH functionalized SBA-16 was used as support.[30] At pH = 9, -COOH and Si-OH deprotonated to -COO- and Si-O- which then attracted Ni^{2+} ions (Scheme 4). In this approach, the Ni particle sizes over Ni supported on -COOH functionalized SBA-16 with loading amount of 5.9, 14.2 and 21.7 wt% were 2.7, 3.6 and 4.7 nm, respectively. Both the intrinsic activity of CO_2 hydrogenation and the selectivity to CH_4 over Ni/SBA-16 functioned with -COOH were higher compared to the results obtain over Ni/SBA-16. To stabilize Ni particles and the SBA-16 framework, 10 wt% Ni was impregnated onto SBA-16 pre-loaded with 10 wt% of Ce.[116] Both Ni and Ce species were highly dispersed over SBA-16, resulting in large amounts of small particles and high $Ce^{3+}/(Ce^{3+} + Ce^{4+})$ ratio. Hence, the activation of CO_2 over Ce^{3+} was enhanced, which then contributed to the increased selectivity to CH_4 over 10 wt% Ni/10 wt% Ce-SBA-16 catalyst compared to 10 wt% Ni/SBA-16 catalyst.[117]
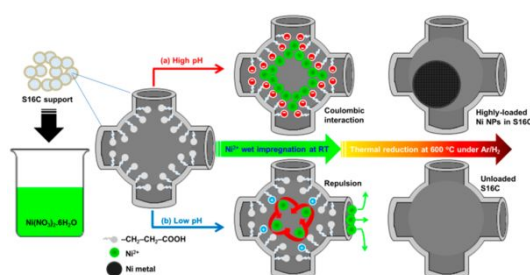
Scheme 4. Synthesis of Ni(x)@S16C Under (a) Basic (with Formation of Ni NPs) and (b) Acidic (without Formation of Ni NPs) Conditions. (Reproduced from ref. 30 with permission from American Chemical Society, copyright 2017)

The selectivity to CH_3OH can be dramatically improved over Cu catalysts. However, the decrease in the metallic surface area due to the sintering of metallic Cu particles is the most significant problem for catalyst deactivation. Thus, essential components such as Zn are incorporated into the catalysts (Cu-Zn-Al) to stabilize Cu, which are extensively used for synthesis of methanol from syngas in industry. Confining Cu particles in the mesopores is also a popular choice to address the sintering problem.[118] Cu-Zn-ZrO$_2$/SBA-15 catalysts were prepared by impregnation-sol-gel auto-combustion method.[102] The high specific surface area of SBA-15 facilitated the dispersion of active phases and contributed to the large surface area of Cu-MO$_x$ (M = Zn and/or Zr) interface. Moreover, the surface inside the pores formed a homogeneous nanolayer with Zn species, which increased the interaction between Cu and MO$_x$. Consequently, the formation rate of CH_3OH over the SBA-15 supported catalysts (158-376 $mg_{CH_3OH} \cdot h^{-1} \cdot g_{cat}^{-1}$) was higher than that obtained on unsupported catalysts (10 $mg_{CH_3OH} \cdot h^{-1} \cdot g_{cat}^{-1}$). As the reaction produced a significant amount of water (CH_3OH/H_2O molar ratio = 1), the thick silica wall of SBA-15 was very stable under steam condition. A similar approach is also reported in the hydrogenation of CO_2 to CH_3OH over Cu-LaO$_x$/SBA-15 catalysts.[101] SBA-15 was used to disperse and confine LaO$_x$ and Cu species in the mesopores to maximize surface area of Cu-LaO$_x$ interface, where formate (HCOO*) formed and was subsequently hydrogenated to CH_3OH (Scheme 5).
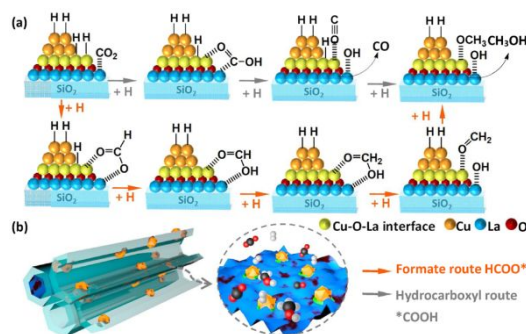
Scheme 5. Proposed reaction mechanism for CO_2 hydrogenation over $Cu_1La_{0.2}$/SBA-15 catalyst. (Reproduced from ref. 101 with permission from Elsevier, copyright 2019)

3.2 Selective hydrogenation

Selective hydrogenation of unsaturated bonds (*e.g.* C=O, N=O) can provide a variety of important bulk chemicals and fines chemicals. One representative example is the selective hydrogenation of C=O in α, β-unsaturated aldehydes (*e.g.* cinnamaldehyde, crotonaldehyde) to produce unsaturated alcohols, which are widely used for industrial preparation of perfumes, flavors, and pharmaceuticals. However, the hydrogenation of the C=C bond is thermodynamically preferred due to the lower bond energy of C=C (615 kJ/mol) compared to C=O (715 kJ/mol).[119] Thus, considerable efforts have been spent to design efficient catalysts to inhibit the hydrogenation of C=C and facilitate the hydrogenation of C=O (**Table 3**). Nobel metals (*e.g.* Pt, Ru, Au and Rh) are the most extensively used catalysts because of their excellent activities and/or selectivities to unsaturated alcohols.[120,121] The selective hydrogenation of α, β-unsaturated aldehydes is highly dependent on the size of noble metal particles because the fraction of exposed facets, steric hindrance of the C=C bond, and poisonous CO generated from decarbonylation reaction are influenced by particles sizes.[122,123]

Table 3. Applications of mesoporous silica-based catalysts in selective hydrogenation.

Materials	Preparation method	Specific surface area (m^2/g)	Pore size(nm)	Pore volume(cm^3/g)	Catalytic reactions	Reaction conditions	Key results	Ref.
Pt/Zn-MCM-41	Impregnation	~	~	~	Hydrogenation of crotonaldehyde	80 ºC, H$_2$/crotonaldehyde ratio =26, H$_2$ flowrate: 50 ml/min, atmospheric pressure, 100 mg of catalyst	Conversion = 4 %, selectivity to crotyl alcohol =37% over Pt/Zn-MCM-41(0.8wt% Pt,	124

							1.98wt% Zn)	
Cu/MCM-48	Hydrother-mal method	423	3.7	~	Hydrogenation of crotonaldehyde	200 mg of catalysts, batch reaction at 100 °C and 1MPa H_2, 0.1M solution of crotonaldehyde in iso-propanol	Selectivity to crotyl alcohol=55% at 10% of conversion (5.5wt% Cu/MCM-48)	125
Ag/MCM-41	Deposition-precipitation method	266	6.37	0.46	Hydrogenation of dimethyl oxalate (DMO) to methyl glycolate	15 wt.% DMO in methanol, H_2/DMO = 100, 2.5 MPa, 220 °C, LHSV =0.2 h^{-1}, 2 g of catalyst	Conversion of DMO =95%, selectivity to methyl glycolate = 95% over 10 wt%Ag/MCM-41	126
Ru–Au/MCM-41	Impregnation	850.67	3.73	0.80	Hydrogenation of Cinnamaldehyde	50 mg of catalyst, 0.5 g of CALD, 20 mL ethanol, T=70 °C, 3.0 MPa H_2	Conversion of Cinnamaldehyde =60%, selectivity to cinnamyl alcohol = 80%	127
PdAg/MCM-41	Deposition-precipitation	804	3.7	0.7	Hydrogenation of cinnamaldehyde	100 mg of catalyst, 1.0 g of CALD, 20 mL of cyclohexane solvent, 110 °C, 1 MPa H_2, and 2 h	Conversion>99.9%, selectivity to Hydrocinnamaldehyde: 98.6%, over Pd-0.3Ag/MCM-41	128
Pt–Mo_2N/SBA-15	Sodium borohydride (NaBH4) method	350	7.5	0.59	Hydrogenation of cinnamaldehyde	50 mg of the catalyst, 1.00 g of CAL, 30 mL of isopropanol, 1 MPa H_2, 80 °C, 2 h	Conversion of cinnamaldehyde: 85.8%, selectivity to cinnamyl alcohol: 78% over 3 wt% Pt–Mo_2N/SBA-15, TOF: 423 h^{-1}	129

CuPt$_x$/SBA-15	Impregnation	~	~	~	Hydrogenation of cinnamaldehyde	0.1 g of catalyst, 5 wt% Cu in CuPt$_x$/SBA-15, 6 mmol cinnamaldehyde in isopropanol, 102 °C, 37.5 bar, 2.5 h.	Conversion of cinnamaldehyde: 40%, selectivity to cinnamyl alcohol:63% over CuPt$_{0.005}$/SBA-15.	130
Ni–B/SBA-15	Reductant-impregnation method	367.0	6.47	0.482	Hydrogenation of 2-ethylanthraquinone (eAQ)	1.0 g of catalyst, Concentration of eAQ = 50 g/L , 50 °C, 0.3 MPa H$_2$, r$_s$ = 1000 rpm	Percent yield of H$_2$O$_2$:100% at 90 min	131
Pd-MS-50-TMB	Co-condensation	854	3.8	1.06	Hydrogenation of chloronitrobenzenes (CNB)	2.5 g of p-CNB, 0.05 g of catalyst, 85 °C and 3.45 MPa of H$_2$, 2 h	Conversion of p-CNB=100 %, selectivity to p-chloroaniline = 99.9%	132
Ni-Co/SBA-15	Impregnation	406.3	7.53	0.88	Hydrogenation of furfural	0.8 g of catalyst, 5 ml (5.82 g) of furfural and 50 ml (39.68 g) of ethanol, 90 °C, 50 bar of initial H$_2$, 2.0 h	100% of FFR con-version and 92.1% of THFA selectivity over Ni-Co/ SBA-15 (Ni/Co molar ratio:0.67)	133

Pt nanoparticles with different sizes were anchored in SBA-15 by encapsulation method.[122] Both the intrinsic activity of crotonaldehyde hydrogenation and the selectivity to unsaturated alcohol in gas phase increased when particle sizes of Pt increased from 1.7 nm to 7.1 nm. However, the hydrogenation of cinnamaldehyde in liquid phase over Pt/SBA-15 and Pt/SiO$_2$ was found to be structure-insensitive, while the high selectivity to cinnamyl alcohol required large Pt particles.[123],[134] AgIn/SBA-15 was prepared by a modified "two solvent" method with an excess volume of aqueous solution to facilitate the introduction of metals into the channels of SBA-15.[135] Compared to Ag/SBA-15, In species improved the dispersion of Ag and hence the Ag particle size was around 3.4 nm over bimetallic catalysts (Figure 5). The selectivity to crotyl alcohol was 87% over AgIn/SBA-15, much higher than the selectivity over Ag/SBA-15 (54%) in the selective hydrogenation of crotonaldehyde at the given condition. The increase in selectivity to crotyl alcohol was attributed to the smaller Ag particles providing a large amount of coordinatively unsaturated sites and existence of In$_2$O$_3$ as Lewis acid sites for the adsorption of C=O *via* the terminal oxygen atom (η_1-on-top mode).
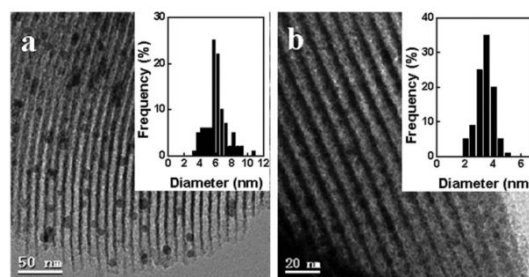
Figure 5. TEM images and particle size distribution histograms (insets) of (a) Ag/SBA-15 and (b) Ag–In/SBA-15 fabricated by the modified ''two solvents'' strategy recorded along the [110] zone axis of SBA-15. (Reproduced from ref. 135 with permission from The Royal Society of Chemistry, copyright 2011)

Moreover, the properties of support also influenced the selectivity to unsaturated alcohol.[136] Pt/SBA-15 was more selective to cinnamyl alcohol than Pd/SiO$_2$ with the same particle sizes.[134] DRIFT studies revealed that the density of surface silanols over SBA-15 was almost twice of surface silanols density on fumed silica (3.0 vs. 1.6 mmol/g, respectively) (Figure 6). The silanols over SBA-15 were geminal/vicinal types, while only isolated silanols existed over fumed silica. These characteristics made SBA-15 more polar than fumed silica and disfavored the adsorption of cinnamaldehyde and cinnamyl alcohol over Pt *via* C = C (di-σ$_{CC}$), as it required orienting the nonpolar phenyl ring close to the support surface. Instead, the adsorption of cinnamaldehyde *via* C=O (di-σ$_{CO}$) is favored as the molecular plane was tilted away from the support surface.
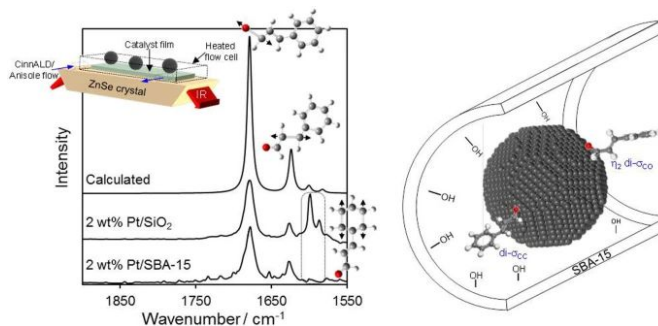
Figure 6. (left) *In situ* ATR-IR spectra of 2 wt% silica supported Pt catalysts films under a flowing CinnALD/anisole solution at 90°C and (right) illustration of unfavorable aromatic-surface interaction arising from adoption of di-σ$_{CC}$ versus di-σ$_{CO}$ CinnALD adsorption on platinum nanoparticles within polar SBA-15 pores. (Reproduced from ref. 134 with permission from Springer Nature, copyright 2015)

Reducible supports (*e.g.* TiO$_2$, CeO$_2$, Fe$_2$O$_3$) are widely applied for the selective hydrogenation of α, β-unsaturated because the interaction between supports and metals can provide interesting changes such as modifying surface electronic properties of metals and suppressing the migration of metal particles on the support surface.[119] However, the specific surface area of these reducible oxides is typically very low. Dispersing them onto supports with large specific surface area, such as ordered mesoporous silica, and then loading metal particles onto support might overcome that disadvantage. 15 wt% TiO$_2$@SBA-15 (15TS) was prepared by hydrolysis of tetrabutyl titanate (TBT)

over SBA-15 and then 5 wt% Pt/15TS and 5 wt% Pt/15TS doped with 0.36 wt% Fe were prepared by impregnation method (Figure 7).[119] The TOF of cinnamaldehyde hydrogenation was much higher over 5 wt% Pt/15TS (0.41 s^{-1}) compared to 5 wt% Pt/TiO$_2$ (0.28 s^{-1}) and 5 wt% Pt/SBA-15 (0.18s^{-1}) under given condition, possibly due to the interaction between Pt particles and a thin layer of highly dispersed and amorphous TiO$_2$ over SBA-15. The TOF increased to 1.36 s^{-1} when impregnating 0.36 wt% Fe to 5 wt% Pt/15TS. Both the conversion of cinnamaldehyde and selectivity to cinnamyl alcohol increased over PtFe/15TS (5 wt%Pt, 0.36 wt% Fe) compared to 5 wt%Pt/15TS. Elevating the calcination temperature of PtFe/15TS(5 wt%Pt, 0.36 wt% Fe) could further increase the TOF and selectivity to cinnamyl alcohol. The positive role of Fe species was attributed to an interaction between Pt and FeO$_x$ which caused electron-deficient Pt$^{\delta+}$ species and Fe^{2+} species for the activation of carbonyl.
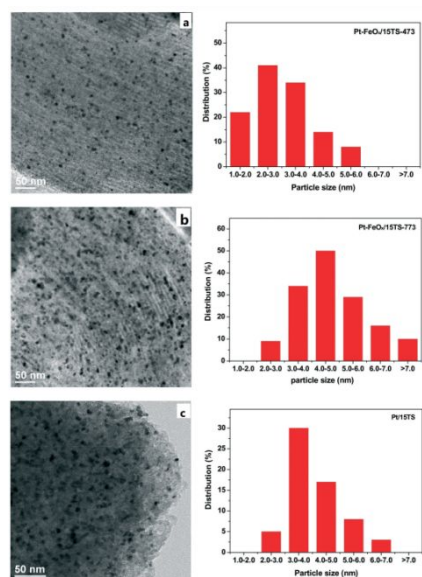
Figure 7. TEM images and particle size distributions of Pt-based catalysts: (a) Pt–FeO$_x$/15TS-473; (b) Pt–FeO$_x$/15TS-773; and (c) Pt/15TS. (Reproduced from ref. 119 with permission from The Royal Society of Chemistry, copyright 2017)

Partly substituting expensive Pt by metal nitrides is investigated as metal nitrides exhibit similar chemical properties as Pt in many catalytic applications. Pt-Mo$_2$N/SBA-15 was prepared by sequential functionalization-nitriding-impregnation method.[129] At the same level of TOF, the selectivity to cinnamyl alcohol was 2.5 times that obtained over 3 wt% Pt/SBA-15. Mo$_2$N species not only facilitated the dispersion of Pt but also increased the content of Pt^0 on the surface, which was proposed to account for the improved activity and selectivity to cinnamyl alcohol.

3.3 Dehydrogenation

Dehydrogenation is proposed to produce a variety of unsaturated building blocks (*e.g.* propylene, ethylene, acetaldehyde, styrene) from abundant resources (*e.g.* propane, ethane, ethanol, ethylbenzene) (**Table 4**).[137,138,139,140] Among them, the dehydrogenation of propane is

the most extensively investigated topic as it can provide valuable propylene from excess propane. Direct dehydrogenation of propane is an endothermic and equilibrium-limited reaction requiring high temperature and low pressure. Too-high reaction temperature usually causes problems like cracking, carbon deposition, *etc*. Oxidative dehydrogenation using molecular O_2 is implemented to overcome these problems. In oxidative dehydrogenation, the heat released by the oxidation of abstracted H makes the reaction exothermic. Thus, the reaction can proceed at lower temperature compared with direct dehydrogenation. However, the selectivity to target products decreases at high conversion of reactants due to the oxidation of propylene. Thus, mild oxidants, such as CO_2, N_2O, are used to replace O_2 which influences the product selectivity.

Table 4. Applications of mesoporous silica-based catalysts in dehydrogenation.

Materials	Preparation method	Specific surface area (m^2/g)	Pore size (nm)	Pore volume (cm^3/g)	Catalytic reactions	Reaction conditions	Key results	Ref.
LaVO$_X$/SBA-15	Impregnation	417.3–467.6	5–7	0.62–0.68	Dehydrogenation of ethylbenzene (EB)	600 °C, atmospheric pressure, 0.3 g of catalyst, ethylbenzene: 5 mmol/h, total flowrate: 15 ml/min (molar ratio of CO_2/EB = 10:1)	Conversion of ethylbenzene: 80%, yield of styrene: 74% at TOS of 2h over 10 wt%La$_2$O$_3$ −15 wt%V$_2$O$_5$/SBA-15	137
Fe-MCM-41	One pot synthesis	642	3.9	0.50	Dehydrogenation of ethylbenzene	600 °C, WHSV = 0.7 h^{-1}, 1.5 g of catalyst, Ar/ ethylbenzene molar ratio = 2.5/1.	conversion of ethylbenzene = 32.1 %, selectivity to styrene = 80.1 wt%	141
CrOx/SBA-15	Impregnation	~	~	~	Dehydrogenation of ethane	650 °C, atmospheric pressure, 200 mg of catalyst, 3% C_2H_6 -15% CO_2 balanced with N_2, total flow rate of 30 ml/min	Conversion of ethane: 41.0%, selectivity to ethylene: 91.5% over 3Cr/SBA-700-H at TOS of 10 min.	142

PtSnAl/SBA-15	Impregnation	766	7.6	0.92	Dehydrogenation of propane	590 °C, 0.2 g of catalyst, C_3H_8: Ar = 1:5, WHSV of propane = 2.5 h^{-1}	One-pass propane conversion : 55.9%, propylene selectivity: 98.5% over PtSnAl0.2/SBA-15	143
Sn-HMS	Co-condensation	960	3.11	0.71	Dehydrogenation of propane	600 °C, atmospheric pressure, 1.5 g of catalyst, 167 h^{-1} gas space velocity, propane flow rate: 5 mL/min	Conversion of propane =40%, selectivity to propylene = 90% over 5 wt%Sn-HMS	144
Co-mSiO$_2$	Neutral templating method	880	2.2	0.16	Dehydrogenation of propane	0.5g of catalyst, 10% propane, a propane-to-helium ratio of 1:10 with a total flow rate of 30 mL/min, at 600 °C	Conversion of propane >35%, selectivity to propylene: 70%, over 2wt%Co-mSiO2	145
V-MSNS	Co-condensation	742.99	4.37	1.05	Dehydrogenation of Propane	0.2 g of catalyst, 600 °C, C_3H_8/CO_2/Ar molar ratio = 1/4/4, inlet flow = 15 mL/min, space velocity of 4500 cm^3/(g·h) at 0.1 Mpa	Propane conversion :58%, selectivity to propylene: 82% over 5.2 wt % V-MSNS	146
V-KIT-6	Hydrothermal method and pH adjusting method	846	9.7	1.15	Dehydrogenation of Propane	0.10 g of catalyst, C_3H_6/O_2/N_2 = 1/1/8, total flowrate: 40 ml/min.	Conversion of propane: 55.0%, selectivity to propylene: 64.7%, selectivity to ethylene:5.5%, over 5V-KIT-6	147

Cu@mSiO2	Modified Stöber method	164	2.3	0.11	Dehydrogenation of methanol	230 °C, 0.1 MPa, WHSV = 4h^{-1}, n(Ar)/ n(CH$_3$OH) = 3.7	Conversion of methanol: 40%, selectivity to methyl formate: 86% over 7 wt%Cu@mSiO$_2$	148
Cu/MCM-41	One-pot synthesis	606	2.7	0.76	Dehydrogenation of ethanol	0.3 g of catalyst, 300 °C, contact time (W/F) of 16,700 g·s/mol, He flowrate: 5 mL/min.	Conversion of ethanol: 50%, selectivity to acetaldehyde:100% over 2.1wt% Cu/MCM-41-pH7-30 °C	149

Pt- and Cr-based catalysts show very good activity for propane dehydrogenation. However, Pt is also active for hydrogenolysis reactions, which lead to the deactivation by carbon deposition. Thus, different promoters (*e.g.* Sn, Cu, Zn, La, Ce, Na, K, Mg) and supports (*e.g.* SiO$_2$, Al$_2$O$_3$, zeolites, mixed metal oxides) are studied for dehydrogenation of propane over Pt catalysts.[150,151,152] PtSn/Al$_2$O$_3$ and PtSn/ZnO-Al$_2$O$_3$ are commercialized for dehydrogenation of propane.[153,154,155] It is observed that Sn could cover the acidic sites of Al$_2$O$_3$ and suppress side reactions, such as hydrogenolysis and cracking. Although it is still controversial about geometric and/or electronic effects of Sn, it is found that the most of Sn species remain in oxidized form over Al$_2$O$_3$ due to the strong interaction between Sn species and Al$_2$O$_3$ and these oxidized Sn species can improve the dispersion of Pt species.[156] Because the interaction between Pt and silica is very weak, the dispersion of Pt over silica is low compared with Al$_2$O$_3$ as support. Moreover, the reduction degree of Sn species over silica is much higher than the counterparts over Al$_2$O$_3$ and it is observed that too high content of Sn alloyed with Pt negatively affects the intrinsic activity of Pt. Thus, pure silica is not regarded as a good support for Pt catalyzed hydrogenation of propane. To enhance the interaction between Pt and the ordered mesoporous silica, metal oxides such as Al$_2$O$_3$ and MgO are incorporated into ordered mesoporous silica.[143,157,158,159] Pt, Sn and Al precursors were simultaneously impregnated onto SBA-15 to prepare PtSn/Al-SBA-15 catalysts.[143] The increasing amount of Al species could decrease the amount of Sn alloyed with Pt and maintain Sn species in oxidized state (Figure 8). However, excess Al$_2$O$_3$ increased the amount of strong acid sites and caused the deactivation of catalyst by coke deposition.
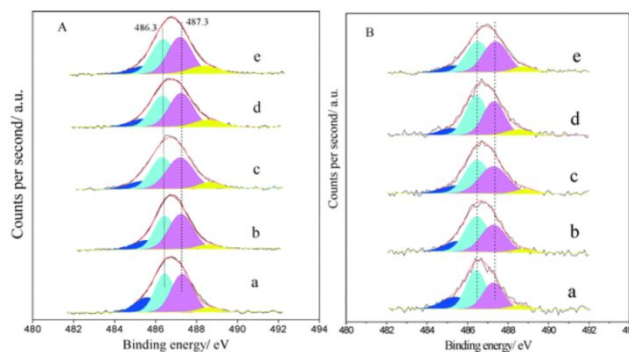
Figure 8. XPS spectra corresponding to Sn $3d_{5/2}$ on reduced PtSnAl/SBA-15 catalysts (A) before reaction and (B) after reaction: (a) PtSnAl$_0$/SBA-15, (b) PtSnAl$_{0.1}$/SBA-15, (c) PtSnAl$_{0.2}$/SBA-15, (d) PtSnAl$_{0.3}$/SBA-15, and (e) PtSnAl$_{0.4}$/SBA-15. Blue: Sn^0 in the Pt–Sn alloy, indigo: Sn^{2+}, purple: Sn^{4+}, yellow: Sn species bound to the support. (Reproduced from ref. 143 with permission from The Royal Society of Chemistry, copyright 2015)

Cr-based catalysts are also used in industry for the direct dehydrogenation of propane as well as oxidative dehydrogenation of propane.[153] Isolated and oligomeric Cr(III)/Cr(II) species are often attributed to the high activity of Cr-based catalysts.[160,161,162,163,164] Different preparation methods and synthesis parameters significantly influence the dispersion and relative content of Cr species.[160,165] Their content on the surface decreases at high loading amount of Cr due to the polymerization of isolated and oligomeric Cr(III)/Cr(II) species. Baek *et al.* observed that isolated Cr(VI) species had a lower reduction temperature than polymeric Cr(VI) species on H_2-TPR profile. The ratio of isolated Cr(VI) species (soft Cr(VI) species) to the total amount of Cr could be correlated with the activity of catalysts (Figure 9).[160] Compared with other supports, ordered mesoporous silica has very high specific surface to disperse Cr species even at high loading amount of Cr.[166] The performance of CrO$_x$/SiO$_2$ catalysts in dehydrogenation of propane with CO$_2$ is better than CrO$_x$/Al$_2$O$_3$ and CrO$_x$/C catalysts.[164] Cr species were reduced in the dehydrogenation of propane. The introduction of oxidants such as O$_2$ and CO$_2$ could partially oxidize the reduced Cr species and suppress the catalyst deactivation.
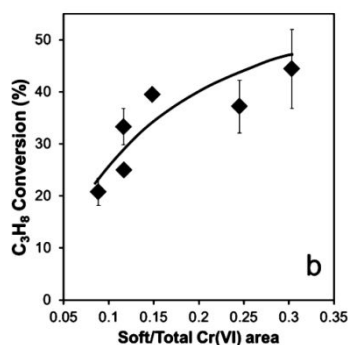

Figure 9. Correlation between the ratio of soft/total Cr(VI) area and the initial ODHP reaction activity of CrMSU-xN catalysts. (Reproduced from ref. 160 with permission from American Chemical Society, copyright 2012)

As Cr(VI) is hazardous, other metal oxides (*e.g.* VO_x, MoO_x, FeO_x, ZnO_x) are studied for dehydrogenation.[138,167,168,169,170,171,172,173] Vanadium oxide and molybdenum oxide-based catalysts are active for alkane dehydrogenation due to their redox properties.[138] Mesoporous silica is used as support for vanadium oxide in the dehydrogenation of propane because of its high specific surface area. The active site for dehydrogenation over supported vanadium oxide is proposed to be isolated tetrahedral vanadium oxide species with terminal V=O groups and oligomeric VO_x species. High dispersion of vanadium oxide is required to obtain these sites. However, the vanadium species tend to form polymerized phase at high loading amount of V (5-10 wt%) and generate active sites for the combustion of hydrocarbons.[168] Thus, the most important aspect for preparing vanadium oxide-based catalysts is increasing the surface concentration of isolated and/or oligomeric VO_x species. Different methods (*e.g.* impregnation, grafting, one-pot synthesis), vanadium precursors (*e.g.* $VOSO_4$, $VOCl_3$, NH_4VO_3, $VO(acac)_2$, $V(t\text{-BuO})_3O$) and supports (*e.g.* MCM-41, SBA-15, KIT-6) were adapted for this aim.[174,175,176] Moreover, the properties of support also influence the dispersion of VO_x species. As V_2O_5 has a point of zero charge (PZC) around 1.4, it interacts weakly with the surface of the support with a low PZC (*e.g.* SiO_2) and thus agglomerates to crystalline V_2O_5.[177] The V-O-Si bonds are sensitive to H_2O formed in the reaction, leading to the disappearance of active species. To enhance the interaction between VO_x and silica surface and isolate VO_x sites, TiO_2, MgO, SbO_x, MoO_x are incorporated to modify the surface properties of silica.[178,179,180,181,182] Hamilton *et al.* prepared $(VO_x)_n$-$(TiO_x)_m$/SBA-15 by a multi-step grafting method. The sub-monolayer TiO_x species promoted the dispersion of VO_x species by forming a VO_x-TiO_x mixed monolayer (Scheme 6). The productivity of propylene reached 5 $g_{propylene}$/(g_{cat}·h) under the reported conditions, which was attributed to the abundance of V-O-Ti bonds.[179]
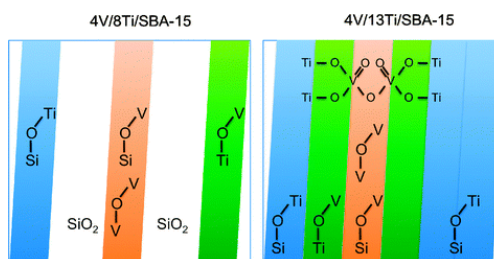
Scheme 6. Schematic illustration of the different surface topologies of V–Ti sub-monolayer catalysts, like 4V/8Ti/SBA-15, and V–Ti monolayer catalysts, like 4V/13Ti/SBA-15, including all topological features evidenced by spectroscopic techniques (white area: free silica surface, blue area: surface area covered by titanium oxide surface species, green area: vanadium oxide species supported on dispersed titania species, orange area: dispersed vanadia species on the silica surface). (Reproduced from ref. 179 with permission from The Royal Society of Chemistry, copyright 2012)

It is proposed that oxidative dehydrogenation of propane over vanadium oxide-based catalysts proceeds *via* Mars-van Krevelen mechanism, in which the reaction between propane and the lattice oxygen of VO_x species produces propene, water and reduced VO_x species.[183] Kinetic research reveals that the reoxidation of VO_x species is fast and the abstraction of H from propane is the rate determining step. The reaction order of O_2 in the oxidative dehydrogenation of propane over supported VO_x catalyst is very low compared with the reaction of propane.[168,184] The selectivity to propene increases when replacing O_2 with N_2O as oxidant. It is attributed to N_2O oxidizing the reduced

VO_x species more slowly than O_2 and thus spatially separating the active oxygen species on the surface.[185] DFT calculations show that the oxidation of reduced VO_x species by N_2O could produce peroxovanadates, which are active for propene combustion.[186] Due to the mild oxidizing ability, peroxovanadates cannot form when using N_2O as oxidant for reduced VO_x species.

3.4 Gas-phase oxidation

Gas phase oxidation over heterogenous catalysts is a typical strategy for pollutants abatement and production of chemicals. The oxidation of CO is extensively investigated because CO is not only an environmental pollutant but also a poison for the Pt catalysts in the fuel cells.[187] Many noble metal (*e.g.* Au, Pt, Ru, Pd, Ag) and non-noble metal (*e.g.* Co, Cu, Fe, Mn) catalysts are active for CO oxidation under various conditions (**Table 5**).[188,189,190,191,192,193] Among them, Au catalysts are the most active and benchmark catalysts for CO oxidation at low temperature. The catalytic activity of Au catalysts is determined by the sizes of Au and metal-support interaction. Au particles with diameter smaller than 5 nm are required to effectively catalyze CO oxidation.[194,195] Compared with supports such as Fe_2O_3, TiO_2 and CeO_2, silica is regarded as inert for Au. The interaction between silica and Au is very weak and silica cannot provide active oxygen for CO oxidation at the Au-SiO_2 interface due to the high bond energy of Si-O. Thus, ordered mesoporous silica is widely used as support to investigate the size effect of Au catalysts in the oxidation of CO as it has narrowly distributed pore system. However, the low interaction between silica and Au also makes it very difficult to prepare Au/SiO_2 catalysts with particle size smaller than 5 nm by common methods. Moreover, the common Au source, $HAuCl_4 \cdot 3H_2O$, becomes $[Au(OH)_x(Cl)_{4-x}]^-$ under typical deposition-precipitation condition (pH=6-10). The surface of silica is negatively charged at that condition due to the low PZC (point of zero charge, < 3) of silica. Thus, surface functionalization of silica with functional groups such as -NH_2, -SH, is employed to load Au particles (< 5 nm) into ordered mesoporous silica.[20,194,196,197] Using positively charged Au sources, such as $[Au(ethylenediamine)_2]^{3+}$, or replacing the Cl^- ligand with NH_3 to form $[Au(NH_3)_{4-x}(OH)_x]^{3-x}$ cations also promotes the interaction of Au with silica surface.[198,199]

Table 5. Applications of mesoporous silica-based catalysts in gas-phase oxidation.

Materials	Preparation method	Specific surface area (m^2/g)	Pore size (nm)	Pore volume (cm^3/g)	Catalytic reactions	Reaction conditions	Key results	Ref.
Ag/HMS	One pot method	1004	2.8	0.92	CO oxidation	200 mg of catalyst, He/CO/O_2 = 79/1/20 at a total flow rate of 30 ml/min.	T_{98} = 20 ºC, over 2.8 wt% Ag/HMS	189
Pd/SBA-15	Impregnation	472	7.7	0.732	CO oxidation	50 mg of catalyst, total flowrate: 20mL/min;1.0 vol.% CO, 20.0 vol.% O_2, balanced with N_2	T_{100} = 135 ºC over H-Pd/SBA-15	200

Cu/SBA-15	Post-grafting	569	5.11	0.79	CO oxidation	60 mg of catalyst, $CO/O_2/H_2/He$ = 1/1/45/53, total flow rate: 20 ml/min	T_{100} = 200 ^oC over 5.7%Cu/SBA-chl	201
Au–Ag/SBA-15	Two-step method	520	7.3	0.95	CO oxidation	60 mg of catalyst, 1.0 vol.% CO and 20 vol.% O_2 balanced with He, total flow rate of 30 ml/min	T_{100} =20 $\circ$C over $Au_{6.0}$-$Ag_{2.0}$/SBA-15	202
Au/Ce/HMS	Deposition–precipitation	760	5.1	1.65	CO oxidation	300 mg of catalyst, CO (1%), O_2 (0.5%), H_2 (0.33%) and N_2 (98.17%), total flow of 100 mL/min	T_{50} = 85 ^oC over 0.67wt%Au/6.8wt%CeO$_2$/HMS catalyst	203
CoNi/mesoporous silica	Organo matrix deposition	490	5.3	0.86	Methane dry reforming	20 mg of catalyst, CH_4:CO_2: He =1:1:8, GHSV = 10,000 mL/(g·h), 700 °C, atmospheric conditions	CH_4 conversion: 89.9%, CO_2 conversion: 90% with a H_2/CO = 1 over 2.5% Co-2.5% Ni/mesoporous silica	204
Ni@SBA-15	One-pot sol-gel method	562	4.0	0.55	Methane dry reforming	50 mg of catalyst, total flowrate: 120 mL/min, GHSV = 144 L/(g·h), 650 °C	CH_4 and CO_2 conversions: ~ 75 %, H_2/CO = ~1 over 5 wt.% Ni@SBA-15	205
Pd@mesoporous silica	Sol-gel process	204.6	7.4	0.535	Methane dry reforming	total flowrate: 60mL/min, CH_4:CO_2:He=1:1:1, atmospheric pressure, 750 °C	CH_4 conversion :83%, CO_2 conversion : 90 %	206
Ni/SBA-15	Solid-state grinding	585	8.1	0.803	Methane dry reforming	50 mg of catalysts, 750 °C, CH_4:CO_2 = 1:1, total flow rate:15 mL/min	CO_2 conversion :64.2%, CH_4 conversion : 53.7% over 23 wt% Ni/SBA-15	9

Ni-KIT-6	One pot method	320.6	17.6	1.41	Methane dry reforming	200 mg of catalyst, 800 ºC, CH_4/CO_2=1:1, GHSV = 1.56×10^4 mL/(g·h), atmospheric pressure .	CO_2 conversion :95%, CH_4 conversion : 85% over 6%Ni-KIT-6	65

Excellent CO oxidation catalysts require the facile activation of O_2 in the reaction as CO could competitively adsorb over the active sites. The activity of Au catalysts is dramatically improved when active supports (*e.g.* Fe_2O_3, TiO_2, CeO_2) are used because small Au particles (<5 nm) can form over the surface of these supports and they have high oxygen storage capacity. However, the specific surface area of these active supports is low compared with ordered mesoporous silica. Thus, dispersing species such as Fe_2O_3, TiO_2 and CeO_2 over the surface of ordered mesoporous silica and then loading Au particles intimately contacting with those species are investigated.[197,207,208,209,210,203,211,212,213,214] A TiO_x monolayer was grafted onto SBA-15 surface and then Au particles were loaded onto the top of TiO_x layer.[209] CO-DRIFTS experiments revealed that Au particles almost exclusively formed over the TiO_x part. The average Au particle size was 3.0 - 4.3 nm with a relatively narrow size distribution over TiO_x modified SBA-15. However, Au particles with size of 6.2 ± 1.9 nm and a broad size distribution formed over pure SBA-15. Consequently, the Au/TiO_x-SBA-15 catalysts was more active than Au/ SBA-15 catalysts in CO oxidation (Figure 10). By increasing the surface coverage of TiO_x while keeping the Au particle size almost constant, the CO oxidation activity increased with TiO_x amount which might be related to surface area of TiO_x species per Au particle. Compared with pure TiO_2 (P25) supported Au catalysts, Au/TiO_x-SBA-15 catalysts did not show improved stability, with a loss in activity of 75-90% during 1000 min on stream. Molecularly adsorbed water contributed to the deactivation of Au/TiO_x-SBA-15 catalysts while other effects, such as reversible reactive modification of the TiO_x layer, also played a role.
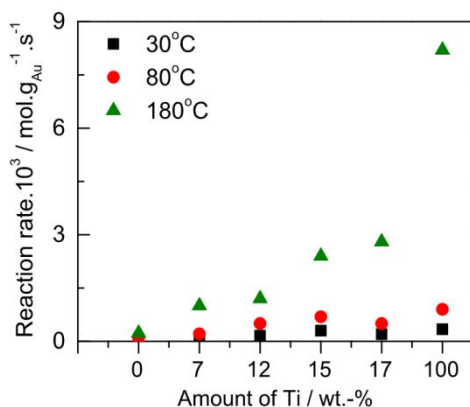

Figure 10. Au mass-normalized initial activities of the different Au/SBA-15-xTicatalysts as a function of Ti wt.% at 30°C, 80°C and 180°C. (Reproduced from ref. 209 with permission from Elsevier, copyright 2017)
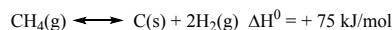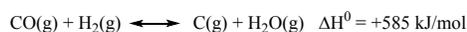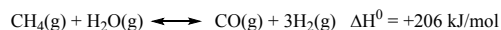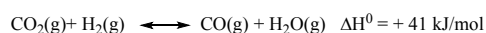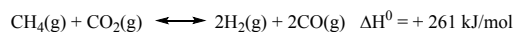
Alloying Au with the other elements with higher oxygen affinity (high element-oxygen bond strength) is also investigated for CO oxidation. The element with higher oxygen affinity would segregate to the surface of the bimetallic particles upon exposure to oxygen in the reaction.

Ag and Cu were able to alloy with Au and provided active oxygen species even over the pure silica supports.[215,216,217,218,219,220] Ag/MCM-41 and Au/MCM-41 showed no or very low catalytic activity in CO oxidation at room temperature.[216] However, 100% CO conversion was achieved over AuAg/MCM-41 catalysts with Au/Ag molar ratio of 3/1 at room temperature. The size effect was ruled out because the average particle sizes were about 20 nm, 6 nm and 20 nm over AuAg/MCM-41, Au/MCM-41 and Ag/MCM-41 catalysts, respectively. The incorporation of Ag facilitated the adsorption of O_2 over the bimetallic sites as EPR revealed that O_2^- species existed over the surface. The results were explained by the synergistic effect between Au and Ag, which accounted for the activation of CO and O_2, respectively (Scheme 7). However, the activity of AuAg/MCM-41 decreased dramatically in the presence of rich H_2 stream, possibly due to the competitive adsorption of H_2 over the metallic sites. By decreasing AuAg particle sizes to 4-6 nm through a modified synthesis method, the as-prepared bimetallic catalyst showed higher activity in CO oxidation at room temperature.[215] AuCu particles were confined in SBA-15 through grafting Au onto APTES-SBA-15 followed by loading of Cu.[218] The incorporation of Cu decreased the metallic particle size over bimetallic catalysts when comparing with Au/SBA-15. The AuCu/SBA-15 was significantly more active and sintering-resistant than Au/SBA-15 and Cu/SBA-15 in CO oxidation. Moreover, the bimetallic catalysts remain active in the presence of excess H_2. *In situ* characterizations revealed that Au^0 and Cu^0 formed Au_3Cu phase while amorphous Cu_2O phase formed between the support and Au_3Cu phase over freshly reduced AuCu/SBA-15. Au tended to segregate into the core of bimetallic phase, leaving the Au surface patched with CuO_x species in CO oxidation.[220] The chemical state of Au was independent on the treatment and remained as Au^0. Au^0 and the CuO_x species served as sites for the activation of CO and O_2, respectively, which was responsible for the high activity of AuCu/SBA-15 in CO oxidation.

$$CO + O_2 + Au\text{-}Ag \rightleftharpoons \overset{CO\ O_2^-}{Au\text{-}Ag^+} \longrightarrow Au\text{-}Ag + CO_2$$

Scheme 7. Proposed mechanism of CO oxidation over Au-Ag catalyst. (Reproduced from ref. 216 with permission from Elsevier, copyright 2005)

Dry reforming of methane (CH_4, DRM) is attractive, as it can consume the two major greenhouse gases (CH_4 and CO_2) and produce syngas with H_2/ CO ratio of about 1 for the downstream application (**Table 5**).[221] As the DRM is highly endothermic, high reaction temperature (600 °C- 900 °C) and low pressure are required. The high operating temperature causes the sintering of metals and many side reactions which decrease the selectivity to syngas and deposit carbon. Kinetic studies show that methane decomposition ($CH4 - s \rightarrow C - s + 2H_2$) is the rate-determining step on the Ni catalysts and the carbon deposition comes from methane dissociation in DRM.[222,223] The main reaction and possible side reactions are list below.[224,225,226]

$$CH_4(g) + CO_2(g) \rightleftharpoons 2H_2(g) + 2CO(g) \quad \Delta H^0 = + 261 \text{ kJ/mol}$$

$$CO_2(g) + H_2(g) \rightleftharpoons CO(g) + H_2O(g) \quad \Delta H^0 = + 41 \text{ kJ/mol}$$

$$CH_4(g) + H_2O(g) \rightleftharpoons CO(g) + 3H_2(g) \quad \Delta H^0 = +206 \text{ kJ/mol}$$

$$CO(g) + H_2(g) \rightleftharpoons C(g) + H_2O(g) \quad \Delta H^0 = +585 \text{ kJ/mol}$$

$$CH_4(g) \rightleftharpoons C(s) + 2H_2(g) \quad \Delta H^0 = + 75 \text{ kJ/mol}$$

$$2CO(g) \rightleftharpoons C(s) + CO_2(g) \quad \Delta H^0 = - 171 \text{ kJ/mol}$$

Noble metals (*e.g.* Ru, Rh, Pd, Pt) and base metals (*e.g.* Ni, Co, Fe) are widely used as the active component of catalysts for DRM.[227,228,229] Noble metals are more resistant to sintering and coke than base metals. They are usually dispersed over metal oxides (*e.g.* Al_2O_3, CeO_2, La_2O_3, ZrO_2) or incorporated as promoters to silica supported base metal catalysts.[227,230] Among the base metal catalysts for DRM, Ni-based catalysts are extensively studied because of their high activity and low cost. However, Ni-based catalysts are prone to sintering and coking. Thus, the investigation of Ni-based DRM catalysts focuses on tuning the properties of Ni by promoters, modifying the properties of support, and developing new synthesis methods.[231,232,233,234] Al_2O_3 is a not good support for Ni because it contributes to the carbon deposition and forming inactive spinel phase.[224] It is observed that carbon deposition could be significantly inhibited when the particle size of Ni is below 7-10 nm.[235] Thus, ordered mesoporous silica with large specific surface area and narrow pore size distribution and large pore volume is a promising support for Ni catalysts.

Apart from noble metals, Mg, La, Sc, Ce, Gd, Co, Mo, *etc.* are effective for promoting the performance of mesoporous silica supported Ni catalysts in DRM.[221,224,226,228,236,237] The roles of promoters are attributed to increasing the basicity of catalysts and enhancing the dispersion of metal species (Figure 11). The increase in basicity can facilitate the adsorption of CO_2 and removing carbon by gasification. For example, XRD and FTIR revealed that La_2O_3 could react with CO_2 to form $La_2O_2CO_3$ with moderate stability. Isotope experiments showed that $La_2O_2CO_3$ could function as a dynamic oxygen pool in the reaction and favor the removal of coke as CO *via* oxidation reactions ($La_2O_2CO_3$ + C* → La_2O_3 + 2CO + *).[231,238,239] The promoters could also act as spacer to improve the dispersion of Ni particles in the reaction.[240] However, the effectiveness of promoters also depends on the specific catalyst components. Co-Ni/SBA-15 catalysts modified by Mg, La and Sc were prepared by impregnation method.[224,240] Ni and Co species were confined in the mesoporous channels over catalysts with Mg and Sc-modified support, which restricted their growth in the reaction. In contrast, the metal species were mainly located on the external surface of La modified SBA-15 and not resistant to sintering.
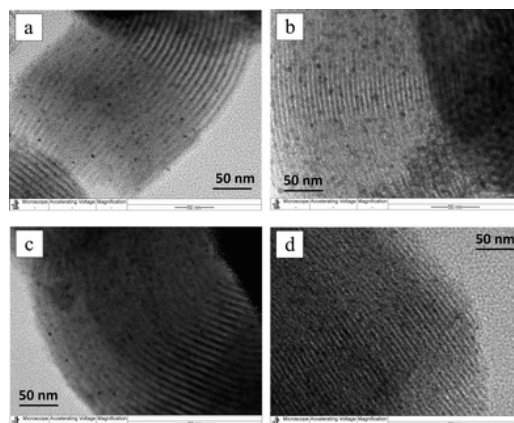
Figure 11. TEM images of reduced Ni/SBA catalysts: (a) 0% La-Ni/SBA, (b) 1% La-Ni/SBA, (c) 2% La-Ni/SBA, and (d) 5% La-Ni/SBA. (Reproduced from ref. 231 with permission from The Royal Society of Chemistry, copyright 2016)

The preparation method significantly influences the distribution of metal species and their interaction.[225] The promoters are usually impregnated onto the support first or co-impregnated with Ni. It is observed that P123 or ultrasonic-assisted impregnation can promote the dispersion of Ni over impregnated catalysts and increase the catalytic stability.[241,242] Albarazi *et al.* compared three preparation methods (sequential impregnation, co-impregnation, co-precipitation) for Ni/SBA-15 promoted by CeO_2-ZrO_2.[232] Less extent of pore blockage, smaller particle size of Ni and stronger interaction between Ni and the support were obtained over catalysts prepared by co-precipitation. Although the formation of nickel phyllosilicate slightly decreased the activity of the catalyst, it increased the stability towards sintering. Sol-gel method is also frequently employed to prepared ordered mesoporous silica supported Ni catalysts.[226,240,243] About 3 nm of Ni particles and highly dispersed CeO_2 species are obtained over 8wt%CeO_2-9wt%Ni/MCM-22 prepared by sol-gel method.[226] The catalyst was stable on stream for more than 60 hours in DRM, at 750 °C with GHSV = 24 L/(g h), CH_4/CO_2 = 1:1.

To enhance the dispersion of nickel species over mesoporous silica, Shi et al. grinded the nickel precursors with template-containing SBA-15 followed by calcination.[9] Benefitting from rich -OH group and the nano-confined space between the silica wall and template, much higher dispersion of Ni species was achieved compared with literature results using other methods. Due to the high dispersion of Ni species, the number of large particles with step/edge sites for carbon deposition decreased, which significantly improved the coking-resistance. Moreover, the high Ni dispersion enhanced the interaction between Ni and support to retard the growth the particles.

3.5 Liquid-phase oxidation

Liquid-phase oxidation of hydrocarbons, alcohols and aldehydes to the corresponding products (*e.g.* alcohol, ketone, aldehyde, carboxylic acid) is a way to provide important fine chemicals for industrial applications.[244,245,246,247] Replacing the traditional, heavily-consumed toxic oxidizing agents (*e.g.* $K_2Cr_2O_7$, $KMnO_4$, organic peroxides) by molecular O_2 or H_2O_2 in solventless condition or using environmental friendly solvent over heterogenous catalysts is desirable in terms of minimizing the environmental impact.

Many metal complexes, metal oxides and noble metal clusters have been applied for the oxidation of alcohol.[245,246,248,249,250,251,252] Metal complexes (*e.g.* Pd complex, Cu complex, Fe complex) are very effective for the transformation, but suffer from the problem of catalyst separation and product contamination.[253,254] Thus, much research has been conducted to immobilize metal complexes onto ordered mesoporous silica due to its large specific surface area and abundant surface silanol groups. The metal salts usually react with ligands (*e.g.* ionic liquid) form metal complexes and then the functional group of the ligand binds with the sinanol on ordered mesoporous silica immobilize the metal complexes.[255] The ordered mesoporous silica can also be functionalized with ligand (*e.g.* N-heterocyclic carbenes) followed by loading metal salts.[256] SBA-15 supported iron-chloride immobilized ionic liquid catalyst was prepared grafting method.[255] The catalysts showed a TON of 125.8 mol/mol$_{Fe}$ in the solvent-free oxidation of benzyl alcohol to benzaldehyde with H_2O_2 as oxidant. A possible mechanism involving the formation of Fe peroxo-complex (I) is shown in Scheme 8.
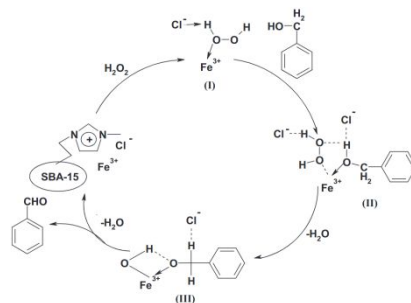
Scheme 8. Proposed reaction mechanism. (Reproduced from ref. 255 with permission from Elsevier, copyright 2015)

It is observed that the supported molecular Pd catalysts are transformed to palladium nanoparticles in the oxidation of alcohol. Yang *et al*. prepared SBA-16 supported Pd-guanidine complex catalyst *via* a one-pot silylation method.[245] Over 99% of selectivity to aldehyde was obtained over the catalyst in the aerobic oxidation of cinnamyl alcohol and benzylic alcohols under an atmospheric pressure of O_2. Pd was coordinated with the ligand over the fresh prepared catalyst but Pd nanoparticles appeared when the reaction started.[257] However, the growth of the Pd nanoparticles was inhibited due to the spatial restriction of the cage structure of SBA-16, which accounted for the excellent recyclability (Scheme 9). Hou *et. al.* found that the SBA-15 supported Pd nanoparticles catalyst had higher activity and stability in aerobic oxidation of benzyl alcohol compared with the SBA-15 supported Pd complexes catalyst.[256] The formation of stable Pd nanoparticles was attributed to the confinement effect of the mesopores on the SBA-15 and N-heterocyclic carbene ligand.
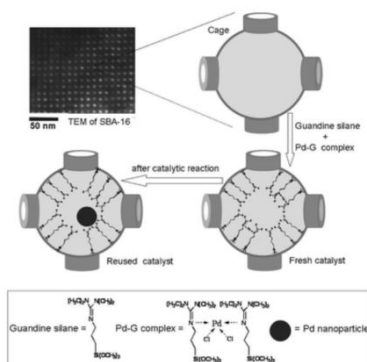
Scheme 9. Schematic descriptions for preparing the solid catalyst Pd-G/SBA-16-G and the model for the reused catalyst. (Reproduced from ref. 245 with permission from The Royal Society of Chemistry, copyright 2010)

Another important category of catalysts for oxidation of alcohols is supported metal catalysts (*e.g*. Au, Pd, Pt, Ru, Co, Mn) (**Table 6**).[258,259,260] An oxidative dehydrogenation mechanism is proposed to explain the liquid-phase oxidation of alcohols over these catalysts, but the detailed pathways are still under debate.[261]

Table 6. Applications of mesoporous silica-based catalysts in liquid-phase oxidation.

Materials	Preparation method	Specific surface area (m^2/g)	Pore size (nm)	Pore volume (cm^3/g)	Catalytic reactions	Reaction conditions	Key results	Ref.
Au–Pd/SBA-15	Grafting method	274	3.4	0.33	Oxidation of benzyl alcohol	Na_2CO_3 aqueous solution (0.55 mol/L, 25 ml), 0.05 ml decane and 0.2 g of catalyst, 0.5 ml of benzyl alcohol, 800 rpm, air atmosphere, 2h, 80 °C	conversion: 20.5%, selectivity to benzaldehyde 98% over Au–Pd/SBA-15	262
Au/mesoporous silica	One pot method	822	4.8	1.3	Oxidation of benzyl alcohol	3.0 g of benzyl alcohol, 50 mg of catalyst, 15 atm oxygen, 130 °C, 1000 rpm, 5h	Conversion of benzyl alcohol: 26.2%, selectivity to benzaldehyde: 98.3%, TOF (mol mol^{-1} (Au) h^{-1}): 377 over 1.5 wt%Au/mesoporous silica	263

3

Au–CeO$_2$@SBA-15	Deposition–reduction	253	4.5	0.25	Oxidation of benzyl alcohol	Benzyl alcohol of 2.5 mmol, catalyst (Au: 0.01 mmol), toluene of 10 mL, O$_2$ flowrate of 20 mL/min, 90 °C, 10 min.	Conversion of benzyl alcohol: 18%, selectivity to benzaldehyde: >99 %, TOF (mol·mol^{-1}(Au) h^{-1}): 270 over 1.97 wt%Au–100CeO$_2$@SBA-15	246
Sulfated Ti-SBA-15	Sol–gel method followed by post synthesis	594	6.6	0.99	Oxidation of benzyl alcohol	0.01 mol of benzyl alcohol, 0.04 mol of hydrogen peroxide (30% w/v), 0.5 g of catalyst, 20 ml of acetonitrile, 60 °C and reaction time of 2 h	Conversion of benzyl alcohol: 62 %, conversioo f H$_2$O$_2$: 70%, selectivity(benzaldehyde): 96% over sulfated Ti-SBA-15 (Si/Ti = 10)	248
Co/SBA-15	Impregnation	~	~	~	Oxidation of ethylbenzene	50 mg of catalyst, 15 ml ethylbenzene, 1.0 MPa O$_2$, 150 °C, 6h	Conversion: 64.5%, selectivity(acetophenone):82.8 %, selectivity (benzoic	264

							acid): 10.4%	
MnO$_x$/SBA-15	Impregnation	481	7.22	0.87	Oxidation of toluene	100 mg of catalyst, 0.235 mol (25 mL) of substrate, 1.0 MPa O$_2$, 180 °C, 1 h	Conversion: 24.7%, selectivity (benzoic acid): 79.5%, selectivity (benzaldehyde): 8.3% over 6 wt% MnO$_x$/SBA-15	265
Au@TiO$_2$/MCM-41	Photocatalytic reduction method	879	2.738	0.69	Oxidation of cyclohexane	8.4 g of cyclohexane, 20 mg of catalyst, 1.0 MPa of O$_2$, 150 °C, 2.5 h	Conversion: 9.79%, selectivity(cyclohexanone): 33.9%, selectivity(cyclohexanol): 34.2%, selectivity(cyclohexyl hydroperoxide): 23.1%,TOF = 28,854 h^{-1} over 0.1wt% Au@TiO$_2$/MCM-41	266
CrO$_x$-MCM-41	Impregnation	859	2.7 and 5.2	0.5	Oxidation of cyclohexane	50 mg of catalyst, 1 mmol of cyclohexane, 70%TBHP (1.2 mmol), CH3CN (5 mL), 70 °C, 24 h	Conversion: 72%, selectivity(cyclohexanone):99% over 5CrO$_x$-MCM-41	267
Nb-MCM-41	One pot method	344	4.1	0.42	Oxidation of 5-hydroxymethylfurfural	1 mmol of HMF, 50 mg of catalysts, 90 °C, CH$_3$CN: 2.5 ml, TBHP: 2 mmol, 12 h	HMF conversion: 93.7 %, DFF selectivity: 99.2 % over Nb-MCM-41(Si/Nb molar ratio:64)	268
Fe/ SBA-1	Impregnation	1175	2.11	0.61	Oxidation of styrene	50 mg of Fe/SBA-1, styrene (1.04 g, 10 mmol), aqueous 30% H$_2$O$_2$ (1.14 g, 10	Conversion: 67 ± 1.49%, selectivity (benzaldeh	269

					mmol), 10 ml of CH$_3$CN, 80 °C, 4 h	yde): 74% over 4 wt% Fe/SBA-1	
					.		

Supported Pd and Au catalysts are intensively studied because of their high catalytic activity. It is observed that the catalytically active species are highly dispersed PdO nanoparticles rather than Pd^0 by kinetic analysis and Pd particles with small size have high intrinsic activity.[270,271,272] The pore architecture influences the dispersion of active sites and mass transfer when using ordered mesoporous silica as support. Remarkable increases in reaction rate were achieved by improving the mesopore connectivity of silica frameworks (amorphous silica, MCM-41, SBA-15, SBA-16, KIT-6), which not only improved mass transport but also increased dispersion of Pd.[271,273] By incorporating complementary macropores (270 nm) into mesoporosity of SBA-15, Parlett *et. al.* found that the dispersion of sub 2 nm Pd nanoparticles was improved, which increased the surface content of PdO as active sites in the oxidation of alcohol. The macropores enabled the bulk reactants (C15-OH and C16-OH) access to active sites and facilitated their conversion.[271] Moreover, the confinement effect of the mesoporous structure enhances the recyclability of the catalyst compared with amorphous silica.[274] To promote the interaction between Pd and support, Al$_2$O$_3$ monolayer was grafted onto SBA-15 before impregnating Pd species.[275] The dispersion of Pd particles was enhanced, which lead to a higher content of surface PdO species. Thus, the Pd/Al-SBA-15 catalyst showed much higher initial activity than Pd/meso-Al$_2$O$_3$ and Pd/SBA-15 in the oxidation of cinnamyl alcohol. The reduction of PdO was identified as one of the reasons for catalyst deactivation and flowing O$_2$ in the reactants could minimize the reduction of PdO.

Supported Au catalysts show unique selectivity to target products compared with other noble metals (Pd, Pt, Ru, *etc*.) in the oxidation of alcohol as over-oxidation is not favored over Au and it can resist strong adsorption of byproducts.[246,276] It is still controversial about the chemical state of Au as active sites.[277,278,279] Similar to other applications of supported Au catalysts, the size of Au nanoparticles determines the intrinsic activity of the catalysts. Smaller Au particles show higher catalytic activity in the oxidation of alcohol.[280,281,282] Liu *et al.* immobilized monodispersed ~1 nm Au clusters within mesoporous channels of SBA-15, MCF and HMS by ligand-protection method.[281,282] The catalysts were active for oxidation of a variety of alcohols in basic medium by H$_2$O$_2$ under microwave irradiation. The dispersion of Au can be improved by incorporating Pd to the catalysts *via* forming Pd-Au alloy, which is attributed the enhanced performance in oxidation of benzyl alcohol to benzaldehyde by O$_2$.[262,276] The agglomeration and leaching of Au are also restricted by the confinement effect of mesoporous structure. However, by confining the Pd-Au nanoparticles in the cage of SBA-16 to form particles with similar size and distribution, Chen *et. al.* attributed the observed enhancement over Pd-Au/SBA-16 in solvent-free aerobic oxidation of benzyl alcohol to the synergetic effect between Au and Pd nanoclusters.[283] Moreover, Wu *et. al*. observed that higher surface PdO content resulted in lower catalytic activity in benzyl alcohol oxidation over PdAu/SiO$_2$ catalyst.[284] The metal-support interaction also plays an important role. Silica supported Au catalysts usually show lower intrinsic activities compared with Au supported over reducible oxides (*e.g.* Fe$_2$O$_3$, CeO$_2$,

3

TiO$_2$) in oxidation reactions because O$_2$ molecules can be activated on the reducible supports or at gold-reducible support interface.[285]

When introducing CeO$_2$ to Au/SBA-15 catalyst in the oxidation of benzyl alcohol, the intrinsic activity over Au-CeO$_2$/SBA-15 showed an increase of about nine-fold and four-fold compared with those over Au/SBA-15 and Au/CeO$_2$ catalysts, respectively.[246] Both Au and CeO$_2$ nanoparticles (~5 nm) were well dispersed in the channel of SBA-15, which generated more Au$^+$ and Ce^{3+} sites on the surface by increasing the interfacial area of Au-CeO$_2$ (Figure 12). The confinement effect of mesoporous channel on Au and CeO$_2$ species resulted in the high stability of the catalyst.
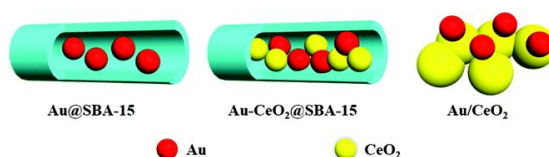

Figure 12. Schematic illustration of the structural system of Au@SBA-15, Au-CeO$_2$@SBA-15 and Au/CeO$_2$ catalysts. (Reproduced from ref. 246 with permission from The Royal Society of Chemistry, copyright 2015)

3.6 Hydrodeoxygenation

Hydrodeoxygenation of oxygenates to fuels or chemicals requires the cooperation between metal sites and acid sites.[286] Transition metals (*e.g.* Pd, Pt, Ru, Ni, Cu, Fe, Co) and their bimetallic combinations are commonly loaded onto support to provide metals sites for C-O bond activation and/or decomposition of H$_2$ (**Table 7**).[286,287,288,289,290] However, pure mesoporous silica is neutral in pH. Thus, surface functionalization of mesoporous silica to incorporate acid sites is a necessary step before introducing other functionalities. Al and Ti are the most frequently used heteroatoms to generate acid sites on mesoporous silica.[289,291,292,293,294] The reaction pathways strongly depend on the acidity of the catalysts as acid sites catalyze the dehydration reaction for the removal of O. The selectivity to products *via* hydrodeoxygenation pathway increases with the Brønsted acidity in the liquid phase hydroprocessing of octanoic acid over Ni/Al-SBA-15 catalysts.[295] However, strong acid sites also facilitate reactions such as cracking, coke deposition, leading to the decrease in the selectivity to target products and catalyst deactivation.[288,295] Thus, the Si/Al or Si/Ti ratio should be tuned in an optimal range to adjust the acid properties of the support.

Table 7. Applications of mesoporous silica-based catalysts in hydrodeoxygenation.

Materials	Preparation method	Specific surface area (m^2/g)	Pore size(nm)	Pore volume(cm^3/g)	Catalytic reactions	Reaction conditions	Key results	Ref.
CuNi/Ti-MCM-41	Impregnation	~	~	~	Hydrodeoxygenation of guaiacol	0.1 g of catalyst, 3 wt% guaiacol, 1 wt% dodecane and 96 wt% heptane, 10 MPa, 260 °C, 6 h with stirring at 1000 rpm	Conversion :~90.49 %, selectivity (cyclohexa	293

						ne):~ 50.09%	
Pt/Nb-KIT-6	Impregnation	~	~	~	Hydrodeoxygenation of guaiacol	50 mg of catalyst, 0.5 MPa, 50 mL/min of H_2, 50 mL/min of N_2, WHSV: 33 h^{-1}, 0.025 mL/min of guaiacol, 400 °C	Conversion: ~90%, selectivity (hydrocarbon): ~75% over a 1 wt % Pt/Nb-KIT-6	296
Pt/Al-SBA-15	Impregnation	229	3.6	~	Hydrodeoxygenation of methoxycyclohexane	25 mg of catalyst, 200 °C, 2 MPa H_2, 10 mmol of methoxycyclohexane, 50 mL of n-dodecane solvent, 800 rpm, and 6 h	Conversion: 100%, selectivity(cyclohexane):95% over 0.16 wt% Pt/Al-SBA-15	297
Co/SBA-15	Impregnation	550	8.8	0.88	Hydrodeoxygenation of anisole	500 mg of catalyst, 0.1 Mpa, 300 °C, LHSV: 20 h^{-1}, 5 wt % anisole in heptane.	Conversion: 62%, selectivity(benzene):71% over 5.3 wt% Co/SBA-15	298
Ni/Al-SBA-15	Impregnation	453	4.1	0.63	Hydrodeoxygenation of octanoic acid	260 °C, 4 MPa H_2 and 150 mg of catalyst in 30 ml reactant (2.5 mmol octanoic acid in dodecane solution)	Conversion: 95%, selectivity(n-C8): 74% over Ni/Al-SBA-15(Si/Al=50)	295
Pd/Nb-SBA-15	Impregnation	~	~	~	Hydrodeoxygenation of 2,5-dimethyltetrahydrofuran	0.1 g of catalysts, 0.2 g of DMTHF, 6.46 g of n-dodecane, 0.1 g of n-octane, 2 MPa H_2, 180 °C, 1h	Conversion: 13.4%, selectivity(n-hexane):71% over Pd/Nb-SBA-15 (Si/Nb=40)	299
Pd/KIT-6	Impregnation	592	3.44	0.38	Hydrodeoxygenation of vanillin	10 wt.% of vanillin, 100 mg of catalyst, WHSV: 21.2 h^{-1}, 300 °C	Conversion: 98%, selectivity (p-cresol): 94% over 5 wt.% of Pd/KIT-6	300

Pd/Al-SBA-15	Impregnation	766	5.7	~	Hydrodeoxygenation of sunflower oil	2.0 MPa, 0.5 g of reactant, 0.2 g of catalyst, 30 mL n-hexane as solvent, 250 °C	74.4% liquid yield and 72.9% C15–C18 hydrocarbons yield over 5 wt% Pd/Al-SBA-15 (Si/Al=300)	288

Supported transition metal phosphides are also extensively studied in the hydrodeoxygenation.[301] The roles of phosphorous not only electronically and geometrically modifies the properties of metal sites but also increases the acidity of catalysts by generating P-OH species.[302] Small Ni_2P particles with uniform size distribution are confined in the mesopores of SBA-15 over the catalyst prepared by temperature-programmed reduction method (Figure 13).[303] The mesopores of SBA-15 stabilize small-sized Ni_2P particles to prevent their sintering when the samples are prepared at 650 °C as the size of Ni_2P particles outside the channel is more than 3 time larger. Smaller nickel phosphide particles are observed to favor the production of n-octadecane *via* hydrodeoxygenation route in the hydroprocessing of methyl oleate.[304] It is suggested that reducing the size of nickel phosphide can increase the density of square pyramidal Ni sites. However, the TOF increases with the Ni_2P particle size in the deoxygenation of methyl laurate over Ni_2P/SiO_2 catalysts.[305] It is attributed to that stronger interaction between Ni and P for Ni_2P particles with smaller size.
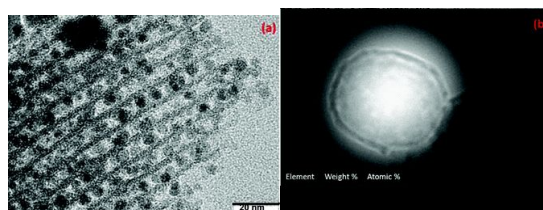

Figure 13. (a) TEM images and (b) TEM−EDX analyses of Ni_2P/SBA15. (Reproduced from ref. 303 with permission from American Chemical Society, copyright 2012)

4. Concluding remarks

Dispersing active species onto supports is a typical method to preparing heterogenous catalysts. Higher dispersion of active species and inhibiting particles growth are two important topics in the catalysis research. Mesoporous silica is characterized by large specific surface area, high specific pore volume, meso-sized pores and abundant silanols on the surface. These properties help to prepare supported catalysts with highly dispersed active species. Locating the particles in the mesoporous channel can prepare catalysts with a narrow distribution of particle size and it is proved as an effective method to improve the catalysts' resistance to sintering. As a neutral support, mesoporous silica cannot provide the acid/base functionalities required by many desired reactions and does not facilitate acid or base catalyzed side

reactions as well. Moreover, the interaction between some active species and the silanol-covered silica surface is week. In this scenario, mesoporous silica is a good scaffold to investigate the interaction between active species and eliminate the size effect. The design of mesoporous silica supported catalysts follows a typical bottom-up strategy. Various functional groups and heteroatoms can be introduced onto mesoporous silica by different methods to modify the properties of mesoporous silica according to applications. These added functionalities can in turn influence the dispersion of active species and interaction between active species and support.

However, functionalization of the surface of mesoporous silica, especially with metal heteroatoms, is still challenging in terms of the efficiency and effectiveness. Unlike zeolites, the acidity of functionalized mesoporous silica is still very limited, which restricts the further applications in related areas. More studies on the introduction of heteroatoms into the framework of mesoporous silica are necessary because it can increase the interaction between active species (*e.g.* noble metals) and support. In addition, the mesoporous structure can offer confinement effect for the particles, but growth of particles along the channel as observed by many researchers can cause the blockage of the channels and result in the less utilization of active sites. The long channels also induce molecular diffusion problem. Thus, adjusting the channel connectivity and channel length of mesoporous silica is an important topic.

Acknowledgement

Reference

1. C. M. Friend and B. Xu, *Accounts of Chemical Research*, 2017, **50**, 517-521.
2. A. J. Bard and M. A. Fox, *Accounts of Chemical Research*, 1995, **28**, 141-145.
3. L. Zhuravlev, *Colloids and Surfaces A: Physicochemical and Engineering Aspects*, 2000, **173**, 1-38.
4. A. Bibby and L. Mercier, *Chemistry of Materials*, 2002, **14**, 1591-1597.
5. A. C. Kresge, M. Leonowicz, W. J. Roth, J. Vartuli and J. Beck, *nature*, 1992, **359**, 710-712.
6. D. Zhao, J. Feng, Q. Huo, N. Melosh, G. H. Fredrickson, B. F. Chmelka and G. D. Stucky, *Science*, 1998, **279**, 548-552.
7. X. Liu, J. Li, L. Zhou, D. Huang and Y. Zhou, *Chemical Physics Letters*, 2005, **415**, 198-201.
8. V. B. Cashin, D. S. Eldridge, A. Yu and D. Zhao, *Environmental Science: Water Research & Technology*, 2018, **4**, 110-128.
9. L. Y. Shi, Y. X. Li, D. M. Xue, P. Tan, Y. Jiang, X. Q. Liu and L. B. Sun, *Chemical Engineering Journal*, 2020, **390**, 124491.
10. L. Y. Shi, Y. X. Li, D. M. Xue, M. Q. Shao, M. X. Gu, X. Q. Liu and L. B. Sun, *Industrial & Engineering Chemistry Research*, 2020, **59**, 19145-19152.
11. Y. Kou and L. B. Sun, *Inorganic Chemistry*, 2018, **57**, 1645-1650.
12. Y. Yin, P. Tan, X. Q. Liu, J. Zhu and L. B. Sun, *Journal of Materials Chemistry A*, 2014, **2**, 3399-3406.
13. E. Serra, Á. Mayoral, Y. Sakamoto, R. M. Blanco and I. Díaz, *Microporous and Mesoporous Materials*, 2008, **114**, 201-213.
14. J. Liang, Z. Liang, R. Zou and Y. Zhao, *Advanced Materials*, 2017, **29**, 1701139.
15. C. Gérardin, J. Reboul, M. Bonne and B. Lebeau, *Chemical Society Reviews*, 2013, **42**, 4217-4255.
16. S. Singh, R. Kumar, H. D. Setiabudi, S. Nanda and D.-V. N. Vo, *Applied Catalysis A: General*, 2018, **559**, 57-74.
17. J. Li, X. Miao, Y. Hao, J. Zhao, X. Sun and L. Wang, *Journal of Colloid and Interface Science*, 2008, **318**, 309-314.
18. X. Xue and F. Li, *Microporous and Mesoporous Materials*, 2008, **116**, 116-122.
19. D. Margolese, J. Melero, S. Christiansen, B. Chmelka and G. Stucky, *Chemistry of Materials*, 2000, **12**, 2448-2459.
20. M. G. Cutrufello, E. Rombi, C. Cannas, M. Casu, A. Virga, S. Fiorilli, B. Onida and I. Ferino, *Journal of Materials Science*, 2009, **44**, 6644-6653.
21. D. Brühwiler, *Nanoscale*, 2010, **2**, 887-892.
22. C. S. Chen, C. C. Chen, C. T. Chen and H. M. Kao, *Chemical Communications*, 2011, **47**, 2288-2290.
23. Y. H. Liu, H. P. Lin and C. Y. Mou, *Langmuir*, 2004, **20**, 3231-3239.
24. B. G. Trewyn, I. I. Slowing, S. Giri, H. T. Chen and V. S. Y. Lin, *Accounts of Chemical Research*, 2007, **40**, 846-853.

25. S. L. Hruby and B. H. Shanks, *Journal of Catalysis*, 2009, **263**, 181-188.
26. S. Ganji, S. Mutyala, C. K. P. Neeli, K. S. R. Rao and D. R. Burri, *RSC Advances*, 2013, **3**, 11533-11538.
27. S. Bagheri, M. M. Amini, M. Behbahani and G. Rabiee, *Microchemical Journal*, 2019, **145**, 460-469.
28. C.-M. Yang, B. Zibrowius and F. Schüth, *Chemical Communications*, 2003, 1772-1773.
29. J. D. Webb, T. Seki, J. F. Goldston, M. Pruski and C. M. Crudden, *Microporous and Mesoporous Materials*, 2015, **203**, 123-131.
30. C. S. Chen, C. S. Budi, H. C. Wu, D. Saikia and H. M. Kao, *ACS Catalysis*, 2017, **7**, 8367-8381.
31. B. Rác, A. Molnar, P. Forgo, M. Mohai and I. Bertóti, *Journal of Molecular Catalysis A: Chemical*, 2006, **244**, 46-57.
32. Y. Yue, A. Gédéon, J. L. Bonardet, J. B. D'Espinose, J. Fraissard and N. Melosh, *Chemical Communications*, 1999, 1967-1968.
33. Y. Li, W. Zhang, L. Zhang, Q. Yang, Z. Wei, Z. Feng and C. Li, *The Journal of Physical Chemistry B*, 2004, **108**, 9739-9744.
34. Z. Y. Wu, H. J. Wang, T. T. Zhuang, L. B. Sun, Y. M. Wang and J. H. Zhu, *Advanced Functional Materials*, 2008, **18**, 82-94.
35. R. Ryoo and M. J. Kim, *Chemical Communications*, 1997, 2225-2226.
36. A. L. de Lima, A. Mbengue, R. A. San Gil, C. M. Ronconi and C. J. Mota, *Catalysis Today*, 2014, **226**, 210-216.
37. X. Y. Liu, L. B. Sun, F. Lu, T. T. Li and X. Q. Liu, *Journal of Materials Chemistry A*, 2013, **1**, 1623-1631.
38. L. Li, K. Quan, J. Xu, F. Liu, S. Liu, S. Yu, C. Xie, B. Zhang and X. Ge, *ACS Sustainable Chemistry & Engineering*, 2013, **1**, 1412-1416.
39. L. Li, K. Quan, J. Xu, F. Liu, S. Liu, S. Yu, C. Xie and X. Ge, *Journal of Analytical and Applied Pyrolysis*, 2014, **110**, 313-317.
40. H. Sun, J. Han, Y. Ding, W. Li, J. Duan, P. Chen, H. Lou and X. Zheng, *Applied Catalysis A: General*, 2010, **390**, 26-34.
41. Y. Huang, S. Xu and V. S. Y. Lin, *Angewandte Chemie International Edition*, 2011, **50**, 661-664.
42. L. Shi, Y. Wang, A. Ji, L. Gao and Y. Wang, *Journal of Materials Chemistry*, 2005, **15**, 1392-1396.
43. V. Antochshuk, A. S. Araujo and M. Jaroniec, *The Journal of Physical Chemistry B*, 2000, **104**, 9713-9719.
44. V. Antochshuk and M. Jaroniec, *Chemistry of Materials*, 2000, **12**, 2496-2501.
45. J. Kecht, A. Schlossbauer and T. Bein, *Chemistry of Materials*, 2008, **20**, 7207-7214.
46. C. M. Yang, H. A. Lin, B. Zibrowius, B. Spliethoff, F. Schüth, S. C. Liou, M. W. Chu and C. H. Chen, *Chemistry of Materials*, 2007, **19**, 3205-3211.
47. C. M. Yang, B. Zibrowius, W. Schmidt and F. Schüth, *Chemistry of Materials*, 2004, **16**, 2918-2925.
48. C. Hernandez and A. Pierre, *Langmuir*, 2000, **16**, 530-536.
49. A. Vinu, V. Murugesan, W. Böhlmann and M. Hartmann, *The Journal of Physical Chemistry B*, 2004, **108**, 11496-11505.
50. R. Mokaya and W. Jones, *Chemical Communications*, 1998, 1839-1840.
51. S. Zeng, J. Blanchard, M. Breysse, Y. Shi, X. Shu, H. Nie and D. Li, *Microporous and Mesoporous Materials*, 2005, **85**, 297-304.
52. F. Chiker, J. P. Nogier, F. Launay and J. Bonardet, *Applied Catalysis A: General*, 2003, **243**, 309-321.
53. P. Wu, T. Tatsumi, T. Komatsu and T. Yashima, *Chemistry of Materials*, 2002, **14**, 1657-1664.
54. Y. Wu, Y. Zhang, J. Cheng, Z. Li, H. Wang, Q. Sun, B. Han and Y. Kong, *Microporous and Mesoporous Materials*, 2012, **162**, 51-59.
55. Y. Li, W. N. Wang, Z. Zhan, M. H. Woo, C. Y. Wu and P. Biswas, *Applied Catalysis B: Environmental*, 2010, **100**, 386-392.
56. E. Rodrıguez-Castellón, A. Jiménez-López, P. Maireles-Torres, D. Jones, J. Roziere, M. Trombetta, G. Busca, M. Lenarda and L. Storaro, *Journal of Solid State Chemistry*, 2003, **175**, 159-169.
57. L. Zhang and J. Y. Ying, *AIChE Journal*, 1997, **43**, 2793-2801.
58. T. Chen, Z. Shi, G. Zhang, H. C. Chan, Y. Shu, Q. Gao and Y. Tang, *ACS Applied Materials & Interfaces*, 2018, **10**, 42475-42483.
59. B. Yang and J. Shi, *Accounts of Materials Research*, 2021, **2**, 581-593.
60. A. Ungureanu, B. Dragoi, A. Chirieac, C. Ciotonea, S. Royer, D. Duprez, A. S. Mamede and E. Dumitriu, *ACS Applied Materials & Interfaces*, 2013, **5**, 3010-3025.
61. A. Rodriguez-Gomez, R. Pereniguez and A. Caballero, *The Journal of Physical Chemistry B*, 2018, **122**, 500-510.
62. X. Yu, M. Burkholder, S. G. Karakalos, G. L. Tate, J. R. Monnier, B. F. Gupton and C. T. Williams, *Catalysis Science & Technology*, 2021, **11**, 2403-2413.
63. Z. Gao and Y. Qin, *Accounts of Chemical Research*, 2017, **50**, 2309-2316.
64. L. Jiao and J. Regalbuto, *Journal of Catalysis*, 2008, **260**, 342-350.
65. Z. Liu, J. Zhou, K. Cao, W. Yang, H. Gao, Y. Wang and H. Li, *Applied Catalysis B: Environmental*, 2012, **125**, 324-330.
66. Z. Taherian, M. Yousefpour, M. Tajally and B. Khoshandam, *International Journal of Hydrogen Energy*, 2017, **42**, 24811-24822.
67. J. Sun, J. Zhang, H. Fu, H. Wan, Y. Wan, X. Qu, Z. Xu, D. Yin and S. Zheng, *Applied Catalysis B: Environmental*, 2018, **229**, 32-40.
68. H. Liu, Y. Li, H. Wu, H. Takayama, T. Miyake and D. He, *Catalysis Communications*, 2012, **28**, 168-173.
69. W. Yang and D. He, *Applied Catalysis A: General*, 2016, **524**, 94-104.
70. W. Yang, H. Liu, Y. Li and D. He, *Microporous and Mesoporous Materials*, 2016, **228**, 174-181.
71. T. Xie, L. Shi, J. Zhang and D. Zhang, *Chemical Communications*, 2014, **50**, 7250-7253.
72. H. Vargas, J. Morales, X. Bokhimi and T. Klimova, *Catalysis Today*, 2018, **305**, 133-142.
73. M. B. Yue, L. B. Sun, Y. Cao, Y. Wang, Z. J. Wang and J. H. Zhu, *Chemistry–A European Journal*, 2008, **14**, 3442-3451.
74. Z. M. Xing, Y. X. Gao, L. Y. Shi, X. Q. Liu, Y. Jiang and L. B. Sun, *Chemical Engineering Science*, 2017, **158**, 216-226.
75. L. Huang, Z. M. Xing, Y. Kou, L. Y. Shi, X. Q. Liu, Y. Jiang and L. B. Sun, *Industrial & Engineering Chemistry Research*, 2018, **57**, 3561-3566.
76. Y. Yin, D. M. Xue, X. Q. Liu, G. Xu, P. Ye, M. Y. Wu and L. B. Sun, *Chemical Communications*, 2012, **48**, 9495-9497.

77.   M. X. Gu, Y. Kou, S. C. Qi, M. Q. Shao, M. B. Yue, X. Q. Liu and L. B. Sun, *ACS Sustainable Chemistry & Engineering*, 2019, **7**, 2837-2843.
78.   X. Y. Liu, L. B. Sun, F. Lu, X. D. Liu and X. Q. Liu, *Chemical Communications*, 2013, **49**, 8087-8089.
79.   L. B. Sun, J. H. Kou, Y. Chun, J. Yang, F. N. Gu, Y. Wang, J. H. Zhu and Z. G. Zou, *Inorganic Chemistry*, 2008, **47**, 4199-4208.
80.   Y. H. Sun, L. B. Sun, T. T. Li and X. Q. Liu, *The Journal of Physical Chemistry C*, 2010, **114**, 18988-18995.
81.   Z. Y. Wu, Q. Jiang, Y. M. Wang, H. J. Wang, L. B. Sun, L. Y. Shi, J. H. Xu, Y. Wang, Y. Chun and J. H. Zhu, *Chemistry of materials*, 2006, **18**, 4600-4608.
82.   X. Y. Liu, L. B. Sun, X. D. Liu, A. G. Li, F. Lu and X. Q. Liu, *ACS Applied Materials & Interfaces*, 2013, **5**, 9823-9829.
83.   A. D. Murkute, J. E. Jackson and D. J. Miller, *Journal of Catalysis*, 2011, **278**, 189-199.
84.   L. B. Sun, X. Y. Liu, A. G. Li, X. D. Liu and X. Q. Liu, *Chemical Communications*, 2014, **50**, 11192-11195.
85.   L. Zhu, F. Lu, X. D. Liu, X. Q. Liu and L. B. Sun, *Chemical Communications*, 2015, **51**, 10058-10061.
86.   Y. Huang, B. G. Trewyn, H. T. Chen and V. S. Y. Lin, *New Journal of Chemistry*, 2008, **32**, 1311-1313.
87.   M. Shokouhimehr, M. S. Asl and B. Mazinani, *Research on Chemical Intermediates*, 2018, **44**, 1617-1626.
88.   T. M. Suzuki, M. Yamamoto, K. Fukumoto, Y. Akimoto and K. Yano, *Journal of Catalysis*, 2007, **251**, 249-257.
89.   T. Yokoi, Y. Kubota and T. Tatsumi, *Applied Catalysis A: General*, 2012, **421**, 14-37.
90.   P. D. Raytchev, A. Bendjeriou, J. P. Dutasta, A. Martinez and V. Dufaud, *Advanced Synthesis & Catalysis*, 2011, **353**, 2067-2077.
91.   L. B. Sun, X. Q. Liu and H. C. Zhou, *Chemical Society Reviews*, 2015, **44**, 5092-5147.
92.   A. R. Silva, K. Wilson, A. C. Whitwood, J. H. Clark and C. Freire, *European Journal of Inorganic Chemistry*, 2006, **2006**, 1275-1283.
93.   F. de Juan and E. Ruiz-Hitzky, *Advanced Materials*, 2000, **12**, 430-432.
94.   N. A. Brunelli, K. Venkatasubbaiah and C. W. Jones, *Chemistry of Materials*, 2012, **24**, 2433-2442.
95.   S. Shylesh, A. Wagner, A. Seifert, S. Ernst and W. R. Thiel, *Chemistry–A European Journal*, 2009, **15**, 7052-7062.
96.   H. K. Lo, I. Thiel and C. Copéret, *Chemistry–A European Journal*, 2019, **25**, 9443-9446.
97.   Q. Sun, X. Fu, R. Si, C. H. Wang and N. Yan, *ChemCatChem*, 2019, **11**, 5093-5097.
98.   S. Rönsch, J. Schneider, S. Matthischke, M. Schlüter, M. Götz, J. Lefebvre, P. Prabhakaran and S. Bajohr, *Fuel*, 2016, **166**, 276-296.
99.   Q. Wang, S. Santos, C. A. Urbina-Blanco, W. Y. Hernández, M. Impéror-Clerc, E. I. Vovk, M. Marinova, O. Ersen, W. Baaziz and O. V. Safonova, *Applied Catalysis B: Environmental*, 2021, **290**, 120036.
100.   S. Kiatphuengporn, M. Chareonpanich and J. Limtrakul, *Chemical Engineering Journal*, 2014, **240**, 527-533.
101.   K. Chen, H. Fang, S. Wu, X. Liu, J. Zheng, S. Zhou, X. Duan, Y. Zhuang, S. C. E. Tsang and Y. Yuan, *Applied Catalysis B: Environmental*, 2019, **251**, 119-129.
102.   M. Mureddu, F. Ferrara and A. Pettinau, *Applied Catalysis B: Environmental*, 2019, **258**, 117941.
103.   Z. Taherian, A. Khataee and Y. Orooji, *Microporous and Mesoporous Materials*, 2020, **306**, 110455.
104.   M. Yang, Z. Lingjun, Z. Xiaonan, R. Prasert and W. Shurong, *Journal of CO$_2$ Utilization*, 2020, **42**, 101304.
105.   X. Wang, L. Zhu, Y. Zhuo, Y. Zhu and S. Wang, *ACS Sustainable Chemistry & Engineering*, 2019, **7**, 14647-14660.
106.   H. Liang, B. Zhang, P. Gao, X. Yu, X. Liu, X. Yang, H. Wu, L. Zhai, S. Zhao and G. Wang, *Chem Catalysis*, 2022, **2**, 610-621.
107.   H. Liu, S. Xu, G. Zhou, K. Xiong, Z. Jiao and S. Wang, *Fuel*, 2018, **217**, 570-576.
108.   N. Koizumi, X. Jiang, J. Kugai and C. Song, *Catalysis Today*, 2012, **194**, 16-24.
109.   Y. Li, H. Zhang, L. Zhang and H. Zhang, *International Journal of Hydrogen Energy*, 2019, **44**, 13354-13363.
110.   J. H. Kwak, L. Kovarik and J. N. Szanyi, *ACS Catalysis*, 2013, **3**, 2449-2455.
111.   J. H. Kwak, L. Kovarik and J. N. Szanyi, *ACS Catalysis*, 2013, **3**, 2094-2100.
112.   G. Du, S. Lim, Y. Yang, C. Wang, L. Pfefferle and G. L. Haller, *Journal of Catalysis*, 2007, **249**, 370-379.
113.   W. L. Vrijburg, J. W. van Helden, A. J. van Hoof, H. Friedrich, E. Groeneveld, E. A. Pidko and E. J. Hensen, *Catalysis Science & Technology*, 2019, **9**, 2578-2591.
114.   M. H. Liu, H. A. Chen, C. S. Chen, J. H. Wu, H.-C. Wu and C. M. Yang, *Nanoscale*, 2019, **11**, 20741-20753.
115.   C. S. Budi, H. C. Wu, C. S. Chen, D. Saikia and H. M. Kao, *ChemSusChem*, 2016, **9**, 2326-2331.
116.   C. Sun, P. Beaunier and P. Da Costa, *Catalysis Science & Technology*, 2020, **10**, 6330-6341.
117.   M. Bacariza, I. Graça, S. Bebiano, J. Lopes and C. Henriques, *Chemical Engineering Science*, 2018, **175**, 72-83.
118.   L. Min, N. Wei, H. C. Ye, H. H. Huo and W. G. Gao, *Journal of Fuel Chemistry and Technology*, 2019, **47**, 1214-1225.
119.   Y. Xue, R. Yao, J. Li, G. Wang, P. Wu and X. Li, *Catalysis Science & Technology*, 2017, **7**, 6112-6123.
120.   J. Hájek, N. Kumar, P. Mäki-Arvela, T. Salmi, D. Y. Murzin, I. Paseka, T. Heikkilä, E. Laine, P. Laukkanen and J. Väyrynen, *Applied Catalysis A: General*, 2003, **251**, 385-396.
121.   X. Yang, D. Chen, S. Liao, H. Song, Y. Li, Z. Fu and Y. Su, *Journal of Catalysis*, 2012, **291**, 36-43.
122.   M. E. Grass, R. M. Rioux and G. A. Somorjai, *Catalysis Letters*, 2009, **128**, 1-8.
123.   A. K. Prashar, S. Mayadevi and R. N. Devi, *Catalysis Communications*, 2012, **28**, 42-46.
124.   J. Silvestre-Albero, J. Serrano-Ruiz, A. Sepúlveda-Escribano and F. Rodríguez-Reinoso, *Applied Catalysis A: General*, 2008, **351**, 16-23.
125.   V. Gutierrez, M. Dennehy, A. Diez and M. A. Volpe, *Applied Catalysis A: General*, 2012, **437**, 72-78.
126.   A. Yin, C. Wen, W. L. Dai and K. Fan, *Applied Catalysis B: Environmental*, 2011, **108**, 90-99.
127.   R. Li, J. Zhao, Z. Gan, W. Jia, C. Wu and D. Han, *Catalysis Letters*, 2018, **148**, 267-276.
128.   R. Li, W. Yao, Y. Jin, W. Jia, X. Chen, J. Chen, J. Zheng, Y. Hu, D. Han and J. Zhao, *Chemical Engineering Journal*, 2018, **351**, 995-1005.

129. D. Wang, Y. Zhu, C. Tian, L. Wang, W. Zhou, Y. Dong, Q. Han, Y. Liu, F. Yuan and H. Fu, *Catalysis Science & Technology*, 2016, **6**, 2403-2412.
130. Y. Cao, J. Guerrero-Sańchez, I. Lee, X. Zhou, N. Takeuchi and F. Zaera, *ACS Catalysis*, 2020, **10**, 3431-3443.
131. X. Chen, S. Wang, J. Zhuang, M. Qiao, K. N. Fan and H. He, *Journal of Catalysis*, 2004, **227**, 419-427.
132. W. Yu, H. W. Lin and C. S. Tan, *Chemical Engineering Journal*, 2017, **325**, 124-133.
133. S. Li, Y. Wang, L. Gao, Y. Wu, X. Yang, P. Sheng and G. Xiao, *Microporous and Mesoporous Materials*, 2018, **262**, 154-165.
134. L. J. Durndell, C. M. Parlett, N. S. Hondow, M. A. Isaacs, K. Wilson and A. F. Lee, *Scientific Reports*, 2015, **5**, 1-9.
135. L. Tian, Q. Yang, Z. Jiang, Y. Zhu, Y. Pei, M. Qiao and K. Fan, *Chemical Communications*, 2011, **47**, 6168-6170.
136. Q. Y. Yang, Y. Zhu, L. Tian, S. H. Xie, Y. Pei, H. Li, H. X. Li, M. H. Qiao and K. N. Fan, *Applied Catalysis A: General*, 2009, **369**, 67-76.
137. B. Liu, G. Rui, R. Chang and C. Au, *Applied Catalysis A: General*, 2008, **335**, 88-94.
138. L. Kong, J. Li, Z. Zhao, Q. Liu, Q. Sun, J. Liu and Y. Wei, *Applied Catalysis A: General*, 2016, **510**, 84-97.
139. C. Autthanit, P. Praserthdam and B. Jongsomjit, *Journal of Environmental Chemical Engineering*, 2018, **6**, 6516-6529.
140. D. S. H. Sam, V. Soenen and J. Volta, *Journal of Catalysis*, 1990, **123**, 417-435.
141. N. Nesterenko, O. Ponomoreva, V. Yuschenko, I. Ivanova, F. Testa, F. Di Renzo and F. Fajula, *Applied Catalysis A: General*, 2003, **254**, 261-272.
142. Y. Cheng, L. Zhou, J. Xu, C. Miao, W. Hua, Y. Yue and Z. Gao, *Microporous and Mesoporous Materials*, 2016, **234**, 370-376.
143. X. Fan, J. Li, Z. Zhao, Y. Wei, J. Liu, A. Duan and G. Jiang, *Catalysis Science & Technology*, 2015, **5**, 339-350.
144. G. Wang, H. Zhang, Q. Zhu, X. Zhu, X. Li, H. Wang, C. Li and H. Shan, *Journal of Catalysis*, 2017, **351**, 90-94.
145. Z. Bian, N. Dewangan, Z. Wang, S. Pati, S. Xi, A. Borgna, H. Kus and S. Kawi, *ACS Applied Nano Materials*, 2021, **4**, 1112-1125.
146. X. L. Xue, W. Z. Lang, X. Yan and Y. J. Guo, *ACS Applied Materials & Interfaces*, 2017, **9**, 15408-15423.
147. Q. Liu, J. Li, Z. Zhao, M. Gao, L. Kong, J. Liu and Y. Wei, *Catalysis Science & Technology*, 2016, **6**, 5927-5941.
148. H. Yang, Y. Chen, X. Cui, G. Wang, Y. Cen, T. Deng, W. Yan, J. Gao, S. Zhu and U. Olsbye, *Angewandte Chemie International Edition*, 2018, **130**, 1854-1858.
149. P. H. Finger, T. A. Osmari, N. M. Cabral, J. M. C. Bueno and J. M. R. Gallo, *Catalysis Today*, 2021, **381**, 26-33.
150. Z. Han, S. Li, F. Jiang, T. Wang, X. Ma and J. Gong, *Nanoscale*, 2014, **6**, 10000-10008.
151. C. Yu, Q. Ge, H. Xu and W. Li, *Applied Catalysis A: General*, 2006, **315**, 58-67.
152. O. A. Bariås, A. Holmen and E. A. Blekkan, *Journal of Catalysis*, 1996, **158**, 1-12.
153. J. J. Sattler, J. Ruiz-Martinez, E. Santillan-Jimenez and B. M. Weckhuysen, *Chemical reviews*, 2014, **114**, 10613-10653.
154. N. Kaylor and R. J. Davis, *Journal of Catalysis*, 2018, **367**, 181-193.
155. Z. Nawaz, X. Tang, Y. Wang and F. Wei, *Industrial & engineering chemistry research*, 2010, **49**, 1274-1280.
156. O. A. Bariås, A. Holmen and E. A. Blekkan, *Catalysis Today*, 1995, **24**, 361-364.
157. B. K. Vu, E. W. Shin, I. Y. Ahn, J. M. Ha, D. J. Suh, W. I. Kim, H. L. Koh, Y. G. Choi and S. B. Lee, *Catalysis letters*, 2012, **142**, 838-844.
158. L. Huang, B. Xu, L. Yang and Y. Fan, *Catalysis Communications*, 2008, **9**, 2593-2597.
159. B. Li, Z. Xu, F. Jing, S. Luo and W. Chu, *Applied Catalysis A: General*, 2017, **533**, 17-27.
160. J. Baek, H. J. Yun, D. Yun, Y. Choi and J. Yi, *ACS Catalysis*, 2012, **2**, 1893-1903.
161. M. Botavina, C. Barzan, A. Piovano, L. Braglia, G. Agostini, G. Martra and E. Groppo, *Catalysis Science & Technology*, 2017, **7**, 1690-1700.
162. S. Derossi, G. Ferraris, S. Fremiotti, E. Garrone, G. Ghiotti, M. Campa and V. Indovina, *Journal of Catalysis*, 1994, **148**, 36-46.
163. K. Takehira, Y. Ohishi, T. Shishido, T. Kawabata, K. Takaki, Q. Zhang and Y. Wang, *Journal of Catalysis*, 2004, **224**, 404-416.
164. I. Takahara, W. C. Chang, N. Mimura and M. Saito, *Catalysis today*, 1998, **45**, 55-59.
165. H. M. Wang, Y. Chen, X. Yan, W. Z. Lang and Y. J. Guo, *Microporous and Mesoporous Materials*, 2019, **284**, 69-77.
166. P. Michorczyk, J. Ogonowski and K. Zeńczak, *Journal of Molecular Catalysis A: Chemical*, 2011, **349**, 1-12.
167. G. Wu, F. Hei, N. Guan and L. Li, *Catalysis Science & Technology*, 2013, **3**, 1333-1342.
168. P. Gruene, T. Wolfram, K. Pelzer, R. Schlögl and A. Trunschke, *Catalysis Today*, 2010, **157**, 137-142.
169. J. Du, H. Xu, J. Shen, J. Huang, W. Shen and D. Zhao, *Applied Catalysis A: General*, 2005, **296**, 186-193.
170. M. Cheng, H. Zhao, J. Yang, J. Zhao, L. Yan, H. Song and L. Chou, *Microporous and Mesoporous Materials*, 2018, **266**, 117-125.
171. K. Chen, S. Xie, A. T. Bell and E. Iglesia, *Journal of Catalysis*, 2000, **195**, 244-252.
172. M. Chen, J. L. Wu, Y. M. Liu, Y. Cao and K. N. Fan, *Catalysis Communications*, 2011, **12**, 1063-1066.
173. A. Ates, C. Hardacre and A. Goguet, *Applied Catalysis A: General*, 2012, **441**, 30-41.
174. J. Santamaría-González, J. Luque-Zambrana, J. Mérida-Robles, P. Maireles-Torres, E. Rodríguez-Castellón and A. Jiménez-López, *Catalysis Letters*, 2000, **68**, 67-73.
175. M. Pena, A. Dejoz, V. Fornes, F. Rey, M. Vazquez and J. L. Nieto, *Applied Catalysis A: General*, 2001, **209**, 155-164.
176. Y. M. Liu, W. L. Feng, T. C. Li, H. Y. He, W. L. Dai, W. Huang, Y. Cao and K. N. Fan, *Journal of Catalysis*, 2006, **239**, 125-136.
177. T. Blasco and J. L. Nieto, *Applied Catalysis A: General*, 1997, **157**, 117-142.
178. R. Monaci, E. Rombi, V. Solinas, A. Sorrentino, E. Santacesaria and G. Colon, *Applied Catalysis A: General*, 2001, **214**, 203-212.

179.   N. Hamilton, T. Wolfram, G. T. Müller, M. Hävecker, J. Kröhnert, C. Carrero, R. Schomäcker, A. Trunschke and R. Schlögl, *Catalysis Science & Technology*, 2012, **2**, 1346-1359.
180.   S. Zhang and H. Liu, *Applied Catalysis A: General*, 2019, **573**, 41-48.
181.   H. Golinska, P. Decyk, M. Ziolek, J. Kujawa and E. Filipek, *Catalysis Today*, 2009, **142**, 175-180.
182.   T. Fu, Y. Wang, A. Wernbacher, R. Schlögl and A. Trunschke, *ACS Catalysis*, 2019, **9**, 4875-4886.
183.   C. Carrero, R. Schlögl, I. Wachs and R. Schomaecker, *ACS Catalysis*, 2014, **4**, 3357-3380.
184.   C. Carrero, M. Kauer, A. Dinse, T. Wolfram, N. Hamilton, A. Trunschke, R. Schlögl and R. Schomäcker, *Catalysis Science & Technology*, 2014, **4**, 786-794.
185.   E. V. Kondratenko, M. Cherian, M. Baerns, D. Su, R. Schlögl, X. Wang and I. E. Wachs, *Journal of Catalysis*, 2005, **234**, 131-142.
186.   X. Rozanska, E. V. Kondratenko and J. Sauer, *Journal of Catalysis*, 2008, **256**, 84-94.
187.   J. Lin, X. Wang and T. Zhang, *Chinese Journal of Catalysis*, 2016, **37**, 1805-1813.
188.   Y. Soni, S. Pradhan, M. K. Bamnia, A. Yadav, S. Jha, D. Bhattacharyya, T. S. Khan, M. Haider and C. Vinod, *Applied Catalysis B: Environmental*, 2020, **272**, 118934.
189.   Z. Qu, X. Zhang, F. Yu and J. Jia, *Microporous and Mesoporous Materials*, 2014, **188**, 1-7.
190.   B. P. Bastakoti, Y. Li, N. Miyamoto, N. M. Sanchez-Ballester, H. Abe, J. Ye, P. Srinivasu and Y. Yamauchi, *Chemical Communications*, 2014, **50**, 9101-9104.
191.   A. Fukuoka, J.-i. Kimura, T. Oshio, Y. Sakamoto and M. Ichikawa, *Journal of the American Chemical Society*, 2007, **129**, 10120-10125.
192.   Á. Szegedi, M. Hegedűs, J. L. Margitfalvi and I. Kiricsi, *Chemical Communications*, 2005, 1441-1443.
193.   C. Tang, J. Sun, X. Yao, Y. Cao, L. Liu, C. Ge, F. Gao and L. Dong, *Applied Catalysis B: Environmental*, 2014, **146**, 201-212.
194.   M. T. Bore, H. N. Pham, E. E. Switzer, T. L. Ward, A. Fukuoka and A. K. Datye, *The Journal of Physical Chemistry B*, 2005, **109**, 2873-2880.
195.   M. Haruta, S. Tsubota, T. Kobayashi, H. Kageyama, M. J. Genet and B. Delmon, *Journal of Catalysis*, 1993, **144**, 175-192.
196.   Y. S. Chi, H. P. Lin and C. Y. Mou, *Applied Catalysis A: General*, 2005, **284**, 199-206.
197.   L. H. Ren, H. L. Zhang, A. H. Lu, Y. Hao and W. C. Li, *Microporous and Mesoporous Materials*, 2012, **158**, 7-12.
198.   P. Kraszkiewicz and W. Mista, *Catalysis Communications*, 2018, **110**, 14-17.
199.   Y. Soni, I. Kavya, T. Ajithkumar and C. Vinod, *Chemical Communications*, 2018, **54**, 12412-12415.
200.   H. Wang and C. J. Liu, *Applied Catalysis B: Environmental*, 2011, **106**, 672-680.
201.   C. H. Tu, A. Q. Wang, M. Y. Zheng, X. D. Wang and T. Zhang, *Applied Catalysis A: General*, 2006, **297**, 40-47.
202.   Z. Qu, G. Ke, Y. Wang, M. Liu, T. Jiang and J. Gao, *Applied Surface Science*, 2013, **277**, 293-301.
203.   J. A. Hernandez, S. Gómez, B. Pawelec and T. Zepeda, *Applied Catalysis B: Environmental*, 2009, **89**, 128-136.
204.   S. Das, M. Sengupta, A. Bag, M. Shah and A. Bordoloi, *Nanoscale*, 2018, **10**, 6409-6425.
205.   O. Daoura, G. Fornasieri, M. Boutros, N. El Hassan, P. Beaunier, C. Thomas, M. Selmane, A. Miche, C. Sassoye and O. Ersen, *Applied Catalysis B: Environmental*, 2021, **280**, 119417.
206.   L. Yue, J. Li, C. Chen, X. Fu, X. Xia, J. Hou, C. Xiao, X. Chen, L. Zhao and G. Ran, *Fuel*, 2018, **218**, 335-341.
207.   C. Peza-Ledesma, L. Escamilla-Perea, R. Nava, B. Pawelec and J. Fierro, *Applied Catalysis A: General*, 2010, **375**, 37-48.
208.   L. Escamilla-Perea, C. Peza-Ledesma, R. Nava, E. Rivera-Muñoz, B. Pawelec and J. Fierro, *Catalysis Communications*, 2011, **15**, 108-112.
209.   G. Kučerová, J. Strunk, M. Muhler and R. J. Behm, *Journal of Catalysis*, 2017, **356**, 214-228.
210.   C. K. Krishnan, K. Nakamura, H. Hirata and M. Ogura, *Physical Chemistry Chemical Physics*, 2010, **12**, 7513-7520.
211.   L. Escamilla-Perea, R. Nava, B. Pawelec, M. Rosmaninho, C. Peza-Ledesma and J. Fierro, *Applied Catalysis A: General*, 2010, **381**, 42-53.
212.   L. Liotta, G. Pantaleo, F. Puleo and A. Venezia, *Catalysis Today*, 2012, **187**, 10-19.
213.   T. Zepeda, A. Martinez-Hernández, R. Guil-López and B. Pawelec, *Applied Catalysis B: Environmental*, 2010, **100**, 450-462.
214.   Y. Li, Y. Guan, R. A. van Santen, P. J. Kooyman, I. Dugulan, C. Li and E. J. Hensen, *The Journal of Physical Chemistry C*, 2009, **113**, 21831-21839.
215.   C. W. Yen, M. L. Lin, A. Wang, S. A. Chen, J. M. Chen and C. Y. Mou, *The Journal of Physical Chemistry C*, 2009, **113**, 17831-17839.
216.   A. Q. Wang, J. H. Liu, S. Lin, T. S. Lin and C. Y. Mou, *Journal of Catalysis*, 2005, **233**, 186-197.
217.   A. Q. Wang, C. M. Chang and C. Y. Mou, *The Journal of Physical Chemistry B*, 2005, **109**, 18860-18867.
218.   X. Liu, A. Wang, X. Wang, C. Y. Mou and T. Zhang, *Chemical Communications*, 2008, 3187-3189.
219.   T. S. Mozer, D. A. Dziuba, C. T. Vieira and F. B. Passos, *Journal of Power Sources*, 2009, **187**, 209-215.
220.   X. Liu, A. Wang, L. Li, T. Zhang, C. Y. Mou and J.-F. Lee, *Journal of Catalysis*, 2011, **278**, 288-296.
221.   R. Mahfouz, J. Estephane, C. Gennequin, L. Tidahy, S. Aouad and E. Abi-Aad, *Journal of Environmental Chemical Engineering*, 2021, **9**, 104662.
222.   A. Luntz and J. Harris, *Surface Science*, 1991, **258**, 397-426.
223.   E. Kuijpers, A. Breedijk, W. Van der Wal and J. Geus, *Journal of Catalysis*, 1983, **81**, 429-439.
224.   A. S. Al-Fatesh, Y. Arafat, H. Atia, A. A. Ibrahim, Q. L. M. Ha, M. Schneider, M. M-Pohl and A. H. Fakeeha, *Journal of CO_2 Utilization*, 2017, **21**, 395-404.
225.   C. Chen, X. Wang, H. Huang, X. Zou, F. Gu, F. Su and X. Lu, *Fuel Processing Technology*, 2019, **185**, 56-67.
226.   R. Amin, X. Chang and B. Liu, *Industrial & Engineering Chemistry Research*, 2017, **56**, 7445-7453.
227.   N. El Hassan, M.-N. Kaydouh, H. Geagea, H. El Zein, K. Jabbour, S. Casale, H. El Zakhem and P. Massiani, *Applied Catalysis A: General*, 2016, **520**, 114-121.
228.   A. S. Al-Fatesh, A. A. Ibrahim, A. H. Fakeeha, S. K. Singh, N. K. Labhsetwar, H. Shaikh and S. O. Qasim, *Renewable Energy*, 2019, **140**, 658-667.

229. L. Qian, W. Cai, L. Zhang, L. Ye, J. Li, M. Tang, B. Yue and H. He, *Applied Catalysis B: Environmental*, 2015, **164**, 168-175.
230. S. Eriksson, S. Rojas, M. Boutonnet and J. Fierro, *Applied Catalysis A: General*, 2007, **326**, 8-16.
231. U. Oemar, Y. Kathiraser, L. Mo, X. Ho and S. Kawi, *Catalysis Science & Technology*, 2016, **6**, 1173-1186.
232. A. Albarazi, M. E. Gálvez and P. Da Costa, *Catalysis Communications*, 2015, **59**, 108-112.
233. M. A. Naeem, A. S. Al-Fatesh, A. E. Abasaeed and A. H. Fakeeha, *Fuel Processing Technology*, 2014, **122**, 141-152.
234. T. Yang, W. Chen, L. Chen, W. Liu and D. Zhang, *Journal of CO$_2$ Utilization*, 2016, **16**, 130-137.
235. J. Zhang, H. Wang and A. K. Dalai, *Applied Catalysis A: General*, 2008, **339**, 121-129.
236. S. Yasyerli, S. Filizgok, H. Arbag, N. Yasyerli and G. Dogu, *International Journal of Hydrogen Energy*, 2011, **36**, 4863-4874.
237. T. Huang, W. Huang, J. Huang and P. Ji, *Fuel Processing Technology*, 2011, **92**, 1868-1875.
238. Z. Zhang, X. E. Verykios, S. M. MacDonald and S. Affrossman, *The Journal of Physical Chemistry*, 1996, **100**, 744-754.
239. L. Qian, Z. Ma, Y. Ren, H. Shi, B. Yue, S. Feng, J. Shen and S. Xie, *Fuel*, 2014, **122**, 47-53.
240. Y. Guo, C. Xia and B. Liu, *Chemical Engineering Journal*, 2014, **237**, 421-429.
241. W. Yang, H. Liu, Y. Li, H. Wu and D. He, *International Journal of Hydrogen Energy*, 2016, **41**, 1513-1523.
242. H. D. Setiabudi, C. C. Chong, S. Abed, L. Teh and S. Chin, *Journal of Environmental Chemical Engineering*, 2018, **6**, 745-753.
243. J. Li, C. Xia, C. Au and B. Liu, *International Journal of Hydrogen Energy*, 2014, **39**, 10927-10940.
244. N. Dimitratos, J. A. Lopez-Sanchez and G. J. Hutchings, *Chemical Science*, 2012, **3**, 20-44.
245. H. Yang, X. Han, Z. Ma, R. Wang, J. Liu and X. Ji, *Green Chemistry*, 2010, **12**, 441-451.
246. T. Wang, X. Yuan, S. Li, L. Zeng and J. Gong, *Nanoscale*, 2015, **7**, 7593-7602.
247. P. Cruz, Y. Perez, I. del Hierro and M. Fajardo, *Microporous and Mesoporous Materials*, 2016, **220**, 136-147.
248. R. V. Sharma, K. K. Soni and A. K. Dalai, *Catalysis Communications*, 2012, **29**, 87-91.
249. P. Wang, Z. Dong, Y. Lei, Y. Du, H. Li, H. Yang, Y. Nie and J. Ma, *Journal of Porous Materials*, 2013, **20**, 277-284.
250. Y. Pérez, R. Ballesteros, M. Fajardo, I. Sierra and I. del Hierro, *Journal of Molecular Catalysis A: Chemical*, 2012, **352**, 45-56.
251. A. L. Cánepa, V. R. Elías, V. M. Vaschetti, E. V. Sabre, G. A. Eimer and S. G. Casuscelli, *Applied Catalysis A: General*, 2017, **545**, 72-78.
252. G. Wu, Y. Gao, F. Ma, B. Zheng, L. Liu, H. Sun and W. Wu, *Chemical Engineering Journal*, 2015, **271**, 14-22.
253. I. E. Marko, P. R. Giles, M. Tsukazaki, S. M. Brown and C. J. Urch, *Science*, 1996, **274**, 2044-2046.
254. I. E. Marko, P. R. Giles, M. Tsukazaki, I. Chelle-Regnaut, A. Gautier, S. M. Brown and C. J. Urch, *The Journal of Organic Chemistry*, 1999, **64**, 2433-2439.
255. R. Cang, B. Lu, X. Li, R. Niu, J. Zhao and Q. Cai, *Chemical Engineering Science*, 2015, **137**, 268-275.
256. Y. Hou, X. Ji, G. Liu, J. Tang, J. Zheng, Y. Liu, W. Zhang and M. Jia, *Catalysis Communications*, 2009, **10**, 1459-1462.
257. B. Karimi, S. Abedi, J. H. Clark and V. Budarin, *Angewandte Chemie International Edition*, 2006, **45**, 4776-4779.
258. K. Yamaguchi, K. Mori, T. Mizugaki, K. Ebitani and K. Kaneda, *Journal of the American Chemical Society*, 2000, **122**, 7144-7145.
259. B. Qi, Y. Wang, L. L. Lou, L. Huang, Y. Yang and S. Liu, *Journal of Molecular Catalysis A: Chemical*, 2013, **370**, 95-103.
260. Y. Li, J. Huang, X. Hu, F. L. Y. Lam, W. Wang and R. Luque, *Journal of Molecular Catalysis A: Chemical*, 2016, **425**, 61-67.
261. M. Besson and P. Gallezot, *Catalysis Today*, 2000, **57**, 127-141.
262. C. Y. Ma, B. J. Dou, J. J. Li, J. Cheng, Q. Hu, Z. P. Hao and S. Z. Qiao, *Applied Catalysis B: Environmental*, 2009, **92**, 202-208.
263. J. Hu, L. Chen, K. Zhu, A. Suchopar and R. Richards, *Catalysis Today*, 2007, **122**, 277-283.
264. H. Ma, J. Xu, C. Chen, Q. Zhang, J. Ning, H. Miao, L. Zhou and X. Li, *Catalysis Letters*, 2007, **113**, 104-108.
265. W. Zhong, S. R. Kirk, D. Yin, Y. Li, R. Zou, L. Mao and G. Zou, *Chemical Engineering Journal*, 2015, **280**, 737-747.
266. J. Zhou, X. Yang, Y. Wang and W. Chen, *Catalysis Communications*, 2014, **46**, 228-233.
267. K. J. Betsy, C. Nayak, A. Lazar, A. Krishnan, D. Bhattacharyya, S. N. Jha and C. P. Vinod, *ChemCatChem*, 2018, **10**, 3291-3298.
268. S. Mahendran, V. Srinivasan, G. Karthikeyan and M. Pachamuthu, *Molecular Catalysis*, 2021, **510**, 111682.
269. W. Tanglumlert, T. Imae, T. J. White and S. Wongkasemjit, *Catalysis communications*, 2009, **10**, 1070-1073.
270. C. M. Parlett, P. Keshwalla, S. G. Wainwright, D. W. Bruce, N. S. Hondow, K. Wilson and A. F. Lee, *ACS Catalysis*, 2013, **3**, 2122-2129.
271. C. M. Parlett, D. W. Bruce, N. S. Hondow, A. F. Lee and K. Wilson, *ACS Catalysis*, 2011, **1**, 636-640.
272. C. H. Liu, C. Y. Lin, J. L. Chen, K. T. Lu, J. F. Lee and J. M. Chen, *Journal of Catalysis*, 2017, **350**, 21-29.
273. Y. Chen, Z. Guo, T. Chen and Y. Yang, *Journal of Catalysis*, 2010, **275**, 11-24.
274. Z. Ma, H. Yang, Y. Qin, Y. Hao and G. Li, *Journal of Molecular Catalysis A: Chemical*, 2010, **331**, 78-85.
275. C. M. Parlett, L. J. Durndell, A. Machado, G. Cibin, D. W. Bruce, N. S. Hondow, K. Wilson and A. F. Lee, *Catalysis Today*, 2014, **229**, 46-55.
276. X. Yang, C. Huang, Z. Fu, H. Song, S. Liao, Y. Su, L. Du and X. Li, *Applied Catalysis B: Environmental*, 2013, **140**, 419-425.
277. H. Kung, M. Kung and C. Costello, *Journal of Catalysis*, 2003, **216**, 425-432.
278. A. Abad, P. Concepción, A. Corma and H. García, *Angewandte Chemie International Edition*, 2005, **44**, 4066-4069.
279. K. Mori, T. Hara, T. Mizugaki, K. Ebitani and K. Kaneda, *Journal of the American Chemical Society*, 2004, **126**, 10657-10666.
280. C. Y. Ma, J. Cheng, H. L. Wang, Q. Hu, H. Tian, C. He and Z. P. Hao, *Catalysis Today*, 2010, **158**, 246-251.
281. Y. Liu, H. Tsunoyama, T. Akita and T. Tsukuda, *Chemistry Letters*, 2010, **39**, 159-161.
282. Y. Liu, H. Tsunoyama, T. Akita and T. Tsukuda, *The Journal of Physical Chemistry C*, 2009, **113**, 13457-13461.
283. Y. Chen, H. Lim, Q. Tang, Y. Gao, T. Sun, Q. Yan and Y. Yang, *Applied Catalysis A: General*, 2010, **380**, 55-65.
284. P. Wu, Y. Cao, L. Zhao, Y. Wang, Z. He, W. Xing, P. Bai, S. Mintova and Z. Yan, *Journal of Catalysis*, 2019, **375**, 32-43.

285.   M. M. Schubert, S. Hackenberg, A. C. Van Veen, M. Muhler, V. Plzak and R. J. Behm, *Journal of Catalysis*, 2001, **197**, 113-122.
286.   T. L. Hewer, A. G. Souza, K. T. Roseno, P. F. Moreira, R. Bonfim, R. M. Alves and M. Schmal, *Renewable Energy*, 2018, **119**, 615-624.
287.   A. Feliczak-Guzik, P. Szczyglewska, M. Jaroniec and I. Nowak, *Catalysis Today*, 2020, **354**, 67-76.
288.   J. Duan, J. Han, H. Sun, P. Chen, H. Lou and X. Zheng, *Catalysis Communications*, 2012, **17**, 76-80.
289.   S. Abd Hamid, M. M. Ambursa, P. Sudarsanam, L. H. Voon and S. K. Bhargava, *Catalysis Communications*, 2017, **94**, 18-22.
290.   A. Szegedi, M. Popova, A. Dimitrova, Z. Cherkezova-Zheleva and I. Mitov, *Microporous and mesoporous materials*, 2010, **136**, 106-114.
291.   N. T. Tran, Y. Uemura, S. Chowdhury and A. Ramli, *Applied Catalysis A: General*, 2016, **512**, 93-100.
292.   S. Gbadamasi, T. H. Ali, L. H. Voon, A. Y. Atta, P. Sudarsanam, S. K. Bhargava and S. B. Abd Hamid, *RSC Advances*, 2016, **6**, 25992-26002.
293.   M. M. Ambursa, P. Sudarsanam, L. H. Voon, S. B. Abd Hamid and S. K. Bhargava, *Fuel Processing Technology*, 2017, **162**, 87-97.
294.   X. Li, J. Zhang, B. Liu, J. Liu, C. Wang and G. Chen, *Fuel*, 2019, **243**, 314-321.
295.   K. B. Baharudin, M. Arumugam, J. Hunns, A. F. Lee, E. Mayes, Y. H. Taufiq-Yap, K. Wilson and D. Derawi, *Catalysis Science & Technology*, 2019, **9**, 6673-6680.
296.   Y. Xiao, A. Ramanathan, B. Subramaniam and A. Varma, *ACS Sustainable Chemistry & Engineering*, 2022, **10**, 4831−4838.
297.   A. Shivhare, J. A. Hunns, L. J. Durndell, C. M. Parlett, M. A. Isaacs, A. F. Lee and K. Wilson, *ChemSusChem*, 2020, **13**, 4945-4953.
298.   Y. Yang, G. Lv, L. Deng, B. Lu, J. Li, J. Zhang, J. Shi and S. Du, *Microporous and Mesoporous Materials*, 2017, **250**, 47-54.
299.   F. Xue, D. Ma, T. Tong, X. Liu, Y. Hu, Y. Guo and Y. Wang, *ACS Sustainable Chemistry & Engineering*, 2018, **6**, 13107-13113.
300.   J. Kayalvizhi and A. Pandurangan, *Molecular Catalysis*, 2017, **436**, 67-77.
301.   G.-N. Yun, A. Takagaki, R. Kikuchi and S. T. Oyama, *Catalysis Science & Technology*, 2017, **7**, 281-292.
302.   V. O. Gonçalves, P. M. de Souza, T. Cabioc'h, V. T. da Silva, F. B. Noronha and F. Richard, *Applied Catalysis B: Environmental*, 2017, **219**, 619-628.
303.   Y. Yang, C. Ochoa-Hernández, V. C. A. de la Peña O'Shea, J. M. Coronado and D. P. Serrano, *ACS Catalysis*, 2012, **2**, 592-598.
304.   Y. Yang, C. Ochoa-Hernández, P. Pizarro, A. Víctor, J. M. Coronado and D. P. Serrano, *Fuel*, 2015, **144**, 60-70.
305.   Y. Yang, J. Chen and H. Shi, *Energy & Fuels*, 2013, **27**, 3400-3409.